


Article

Iron Isotope Compositions of Coexisting Sulfide and Silicate Minerals in Sudbury-Type Ores from the Jinchuan Ni-Cu Sulfide Deposit: A Perspective on Possible Core-Mantle Iron Isotope Fractionation

Peiyao Wang^{1,2,3,*}, Yaoling Niu^{1,2,4,5,*} , Pu Sun^{1,2}, Xiaohong Wang^{1,2}, Pengyuan Guo^{1,2}, Hongmei Gong^{1,2}, Meng Duan^{1,2}, Fangyu Shen^{1,2,3}, Yining Shi⁴, Song Xue⁴, Yanhong Chen⁴ and Li Shan^{1,2,3}

- ¹ Institute of Oceanology, Chinese Academy of Sciences, Qingdao 266071, China; pu.sun@foxmail.com (P.S.); wangxiaohong@qdio.ac.cn (X.W.); guopy@qdio.ac.cn (P.G.); gonghm@qdio.ac.cn (H.G.); m.duan@foxmail.com (M.D.); fangyushen@qdio.ac.cn (F.S.); shanli@qdio.ac.cn (L.S.)
- ² Laboratory for Marine Geology, Qingdao National Laboratory for Marine Science and Technology, Qingdao 266061, China
- ³ College of Earth and Planetary Sciences, University of Chinese Academy of Sciences, Beijing 100049, China
- ⁴ School of Earth Sciences and Resources, China University of Geosciences, Beijing 100083, China; 1001161008@cugb.edu.cn (Y.S.); 1010163118@cugb.edu.cn (S.X.); chenyhlicht@126.com (Y.C.)
- ⁵ Department of Earth Sciences, Durham University, Durham DH1 3LE, UK
- * Correspondence: peiyao.wang@qdio.ac.cn (P.W.); yaoling.niu@durham.ac.uk (Y.N.)



Citation: Wang, P.; Niu, Y.; Sun, P.; Wang, X.; Guo, P.; Gong, H.; Duan, M.; Shen, F.; Shi, Y.; Xue, S.; et al. Iron Isotope Compositions of Coexisting Sulfide and Silicate Minerals in Sudbury-Type Ores from the Jinchuan Ni-Cu Sulfide Deposit: A Perspective on Possible Core-Mantle Iron Isotope Fractionation. *Minerals* **2021**, *11*, 464. <https://doi.org/10.3390/min11050464>

Academic Editors: Dan Asael and Leslie Robbins

Received: 9 March 2021

Accepted: 24 April 2021

Published: 28 April 2021

Publisher's Note: MDPI stays neutral with regard to jurisdictional claims in published maps and institutional affiliations.



Copyright: © 2021 by the authors. Licensee MDPI, Basel, Switzerland. This article is an open access article distributed under the terms and conditions of the Creative Commons Attribution (CC BY) license (<https://creativecommons.org/licenses/by/4.0/>).

Abstract: Many studies have shown that the average iron (Fe) isotope compositions of mantle-derived rocks, mantle peridotite and model mantle are close to those of chondrites. Therefore, it is considered that chondrite values represent the bulk Earth Fe isotope composition. However, this is a brave assumption because nearly 90% of Fe of the Earth is in the core, where its Fe isotope composition is unknown, but it is required to construct bulk Earth Fe isotope composition. We approach the problem by assuming that the Earth's core separation can be approximated in terms of the Sudbury-type Ni-Cu sulfide mineralization, where sulfide-saturated mafic magmas segregate into immiscible sulfide liquid and silicate liquid. Their density/buoyancy controlled stratification and solidification produced net-textured ores above massive ores and below disseminated ores. The coexisting sulfide minerals (pyrrhotite (Po) > pentlandite (Pn) > chalcopyrite (Cp)) and silicate minerals (olivine (Ol) > orthopyroxene (Opx) > clinopyroxene (Cpx)) are expected to hold messages on Fe isotope fractionation between the two liquids before their solidification. We studied the net-textured ores of the Sudbury-type Jinchuan Ni-Cu sulfide deposit. The sulfide minerals show varying $\delta^{56}\text{Fe}$ values (-1.37 – -0.74 ‰ (Po) < 0.09 – 0.56 ‰ (Cp) < 0.53 – 1.05 ‰ (Pn)), but silicate minerals (Ol, Opx, and Cpx) have $\delta^{56}\text{Fe}$ values close to chondrites ($\delta^{56}\text{Fe} = -0.01 \pm 0.01$ ‰). The heavy $\delta^{56}\text{Fe}$ value (0.52 – 0.60 ‰) of serpentines may reflect Fe isotopes exchange with the coexisting pyrrhotite with light $\delta^{56}\text{Fe}$. We obtained an equilibrium fractionation factor of $\Delta^{56}\text{Fe}_{\text{silicate-sulfide}} \approx 0.51$ ‰ between reconstructed silicate liquid ($\delta^{56}\text{Fe} \approx 0.21$ ‰) and sulfide liquid ($\delta^{56}\text{Fe} \approx -0.30$ ‰), or $\Delta^{56}\text{Fe}_{\text{silicate-sulfide}} \approx 0.36$ ‰ between the weighted mean bulk-silicate minerals ($\delta^{56}\text{Fe}_{[0.70\text{ol},0.25\text{opx},0.05\text{cpx}]} = 0.06$ ‰) with weighted mean bulk-sulfide minerals ($\delta^{56}\text{Fe} \approx -0.30$ ‰). Our study indicates that significant Fe isotope fractionation does take place between silicate and sulfide liquids during the Sudbury-type sulfide mineralization. We hypothesize that significant iron isotope fractionation must have taken place during core–mantle segregation, and the bulk Earth may have lighter Fe isotope composition than chondrites although Fe isotope analysis on experimental sulfide-silicate liquids produced under the varying mantle depth conditions is needed to test our results. We advocate the importance of further research on the subject. Given the close Fe-Ni association in the magmatic mineralization and the majority of the Earth's Ni is also in the core, we infer that Ni isotope fractionation must also have taken place during the core separation that needs attention.

Keywords: equilibrium iron isotope fractionation; Jinchuan magmatic sulfide deposit; net-textured sulfide ores; pyrrhotite; chalcopyrite; pentlandite; olivine and pyroxenes; core–mantle Fe isotope fractionation

1. Introduction

The rapid technological development in mass spectrometry has allowed determination of non-traditional stable isotopes of many elements (e.g., Mg, Fe, Cu, Zn, Mo, etc.) in all sorts of Earth materials, which has led to the knowledge that these isotopes do vary on all scales. The question remains whether the observed isotope variation for a given element is inherited from the heterogeneous accretion of our planet or if the variation may have resulted from Earth processes. Our present studies assume uniform bulk Earth isotope composition for a given element, and then interpret isotope variations between minerals, between rocks, and between Earth reservoirs as resulting from Earth processes. It is thus common to read in the literature that isotope variations can be used to constrain Earth processes, but in practice we cannot yet constrain any process before we fully understand the mechanisms of isotope fractionation in response to varying chemical and physical conditions and processes. For this very reason, the iron isotope compositions of the coexisting minerals (e.g., silicates and sulfides) in Sudbury-type ores from the Jinchuan magmatic Ni-Cu sulfide deposit were studied to accumulate observations and to evaluate the possible iron isotope fractionation between the silicate and sulfide liquids prior to the crystallization of these minerals. Importantly, the data and understanding of this work provide a fundamental first step for discussing possible Fe isotope fractionation between the Earth's mantle and its core that hosts almost 90% of the Earth's iron.

Iron (Fe) is the most abundant element in the Earth by mass, and it is also one of the most important multivalent elements (Fe^0 , Fe^{2+} , and Fe^{3+}) in the Earth with four stable isotopes (^{54}Fe (5.84%), ^{56}Fe (91.67%), ^{57}Fe (2.12%), and ^{58}Fe (0.28%)). The observation that iron isotopes of mantle derived melts such as mid-ocean ridge basalts (MORB) and ocean island basalts (OIB) ($\delta^{56}\text{Fe} = 0.11 \pm 0.03\text{‰}$), mantle peridotites ($\delta^{56}\text{Fe} = 0.01 \pm 0.02\text{‰}$), and the estimated fertile upper mantle ($\delta^{56}\text{Fe} = 0.02 \pm 0.03\text{‰}$) [1] have sufficient similarity to those of carbonaceous and ordinary chondrites with a uniform composition ($\delta^{56}\text{Fe} = -0.01 \pm 0.01\text{‰}$) [2–6] has led to the suggestion that carbonaceous chondrites represent the iron isotope composition of the bulk Earth [7]. The implicit assumption is that the Earth's core has the same Fe isotope composition as the silicate Earth and there is no Fe isotope fractionation during the Earth's core separation. However, some studies argued that peridotites are not necessarily representative of the silicate Earth composition and assumed instead that the Earth's mantle as a whole has a heavier iron isotope composition [8]. Beyond that, equating upper mantle iron isotope composition inferred from oceanic basalts and accessible mantle peridotites with chondrite iron isotope composition is very risky because ~87% of Earth's iron is in the core. Any metal-silicate isotope fractionation would significantly affect iron isotopes in the Earth's mantle [9]. Thus, to test the above hypothesis that "carbonaceous chondrite iron isotope composition represents that of the bulk Earth", it is necessary to ascertain the iron isotope composition of the Earth's core, i.e., possible Fe isotope fractionation during the Earth's core separation.

Current research on core–mantle iron isotope fractionation is essentially absent because there is no core material available to study. Some experimental simulations suggest that iron isotope fractionation between silicate and metal phases at different conditions (including those relevant to core formation) is small and negligible (e.g., [10–17]). The most credible approach would be to carry out Fe isotope analysis on sulfide-silicate liquids experimentally produced under the deep mantle conditions. The latter is challenging at present, but we can, as a logical first step, analyze Fe isotopes of naturally occurring sulfide-silicate liquids. The Sudbury-type Ni-Cu-Fe sulfide ores are such materials representing solidified sulfide-silicate liquids resulting from sulfur-rich and sulfide saturated mafic magma segregation. Therefore, we choose to study net-textured ore samples from the Jinchuan magmatic ore deposit, which is the third largest Sudbury-type magmatic Ni-Cu-Fe sulfide ore mineralization. The ore formation process is hypothesized as best approximating the magmatic and physical processes of the Earth's core formation because

of the strong chemical Fe-S and Fe-O bonding before S removal to convert Fe-S into the metallic Fe (Ni and other light elements and trace metals) core of the Earth (detailed in Figure 1).

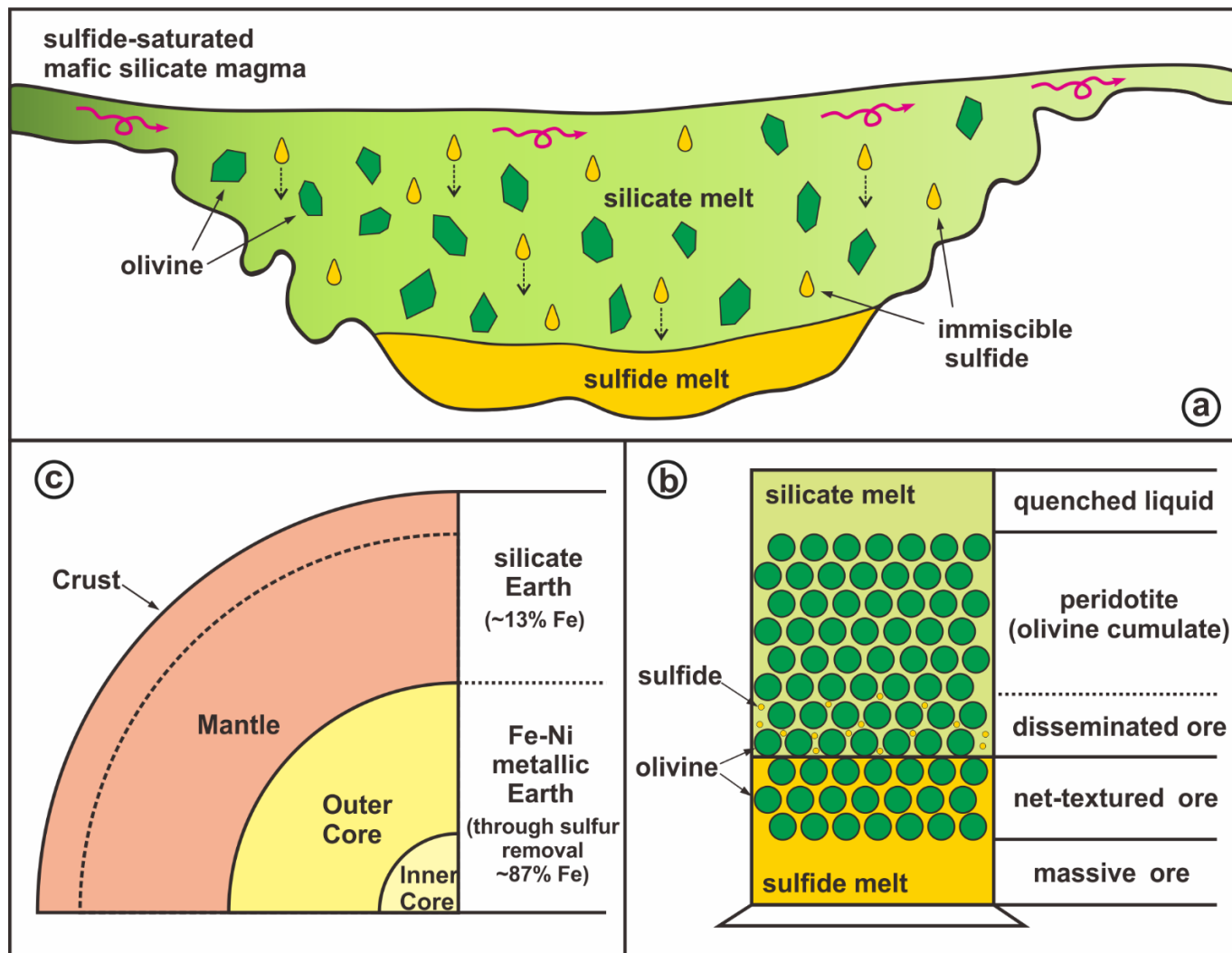


Figure 1. A schematic scenario of magmatic Ni-Cu-Fe sulfide mineralization to illustrate the possible process of core–mantle separation through sulfide-silicate melt segregation. (a) Portion of a cross-section illustrating the silicate-sulfide melt segregation in a magma reservoir relevant to the Sudbury-type sulfide ore mineralization (modified from [18]), where the sulfide-saturated mafic magma segregates to immiscible sulfide liquid from the silicate liquid, and the denser sulfide liquid sinks to the bottom while olivine dominated mafic minerals are crystallizing from the silicate liquid [19]. (b) Continuation of the process in (a), which forms the peridotite of cumulate origin dominated by olivine and varying textured ore types downwards (disseminated, net-textured, and massive ores) as illustrated (modified from [18,20]). (c) While the core is largely metallic (Fe, Ni, etc.), we reason that the core separation must have undergone sulfide-silicate segregation due to density difference, and the sulfide melt must have then developed into metallic core through sulfur removal. As the latter process should not cause iron isotope fractionation, the metallic iron will retain the sulfide liquid iron isotope characteristics. Hence, the net-textured ores showing equilibrium contact between silicates and sulfides provide ideal materials for understanding possible iron isotope fractionation between the metallic core and silicate Earth during core formation. We do not consider the effects of deep mantle pressures and temperatures in this strategically important first step study (see text).

This approach has two assumptions:

- (1) The core separation was accomplished through silicate melt and sulfide melt segregation due to density difference. The sulfide melt must have then developed into the

Fe-Ni metallic core through sulfur removal under core depth pressure-temperature conditions. Hence the prior sulfides and metals must possess the same iron isotope composition, representing that of the metallic core in equilibrium with the silicate Earth (Figure 1).

- (2) The core–mantle separation took place under high pressure and temperature in the deep Earth, but the magmatism takes place under upper mantle or deep crustal conditions. We do not ignore the effects of pressure and temperature on potential Fe isotope fractionation, but we use the best natural materials to study this important problem as the strategically must-do first step. The results will form the foundation for further studies.

In this article, we report the results of our study on Sudbury-type magmatic sulfide ore samples (net-textured and disseminated) from the Jinchuan Ni-Cu sulfide deposit in China, one of the largest Sudbury-type magmatic ore deposits on Earth.

2. Geological Setting

The Jinchuan Ni-Cu sulfide deposit is the third largest magmatic Ni-Cu sulfide deposit next to Sudbury and Noril'sk [21], which contains more than 500 million tons of sulfide ores with an average Ni grade of 1.2 wt.% and Cu grade of 0.7 wt.% [22] plus economically significant PGE metals. The Jinchuan deposit is located east of the Longshoushan uplift belt on the southwestern margin of the North China Craton, with the Alxa block to the north and the North Qilian orogenic belt to the south (Figure 2b), and is divided by multiple faults into four mining areas: III, I, II, and IV from northwest to southeast [23] (Figure 2c). The deposit is hosted in the northwest lenticular mafic-ultramafic intrusive body that intruding the Longshoushan Paleoproterozoic strata. This ore-bearing intrusion is dominated by dunite, harzburgite and lherzolite of cumulate origin with a high degree of serpentinization [24]. The Jinchuan deposit has massive, net-textured and disseminated ores (Figures 1 and 3), consisting of sulfide minerals (pyrrhotite, pentlandite, chalcopyrite, etc.) coexisting with silicate minerals (olivine, clinopyroxene, orthopyroxene, etc.), minor oxide minerals (chromite, magnetite, etc.) and secondary alteration minerals (serpentine, amphibole, chlorite, dolomite, etc.).

Much research has been done on the ore genesis and mineralization age of the Jinchuan deposit. Re-Os isochron ages (833 ± 35 Ma [28]; 1404–1508 Ma [29]), SHRIMP U-Pb ages on zircon and baddeleyite (825–870 Ma [29–31]) and Sm-Nd isochron ages (1508 ± 31 Ma [32]) have been reported in the literature, the U-Pb ages on zircon and baddeleyite (~830 Ma) are thought to be consistent with the break-up of the Rodinia supercontinent. Therefore, the mantle derived magmatism associated with the break-up of the Rodinia supercontinent is considered to be responsible for the Jinchuan ore deposit [30,33–36] although rifting-related intraplate magmatism is also proposed as an alternative on the basis of the geochemistry of metabasite [37] and drill core samples [38].

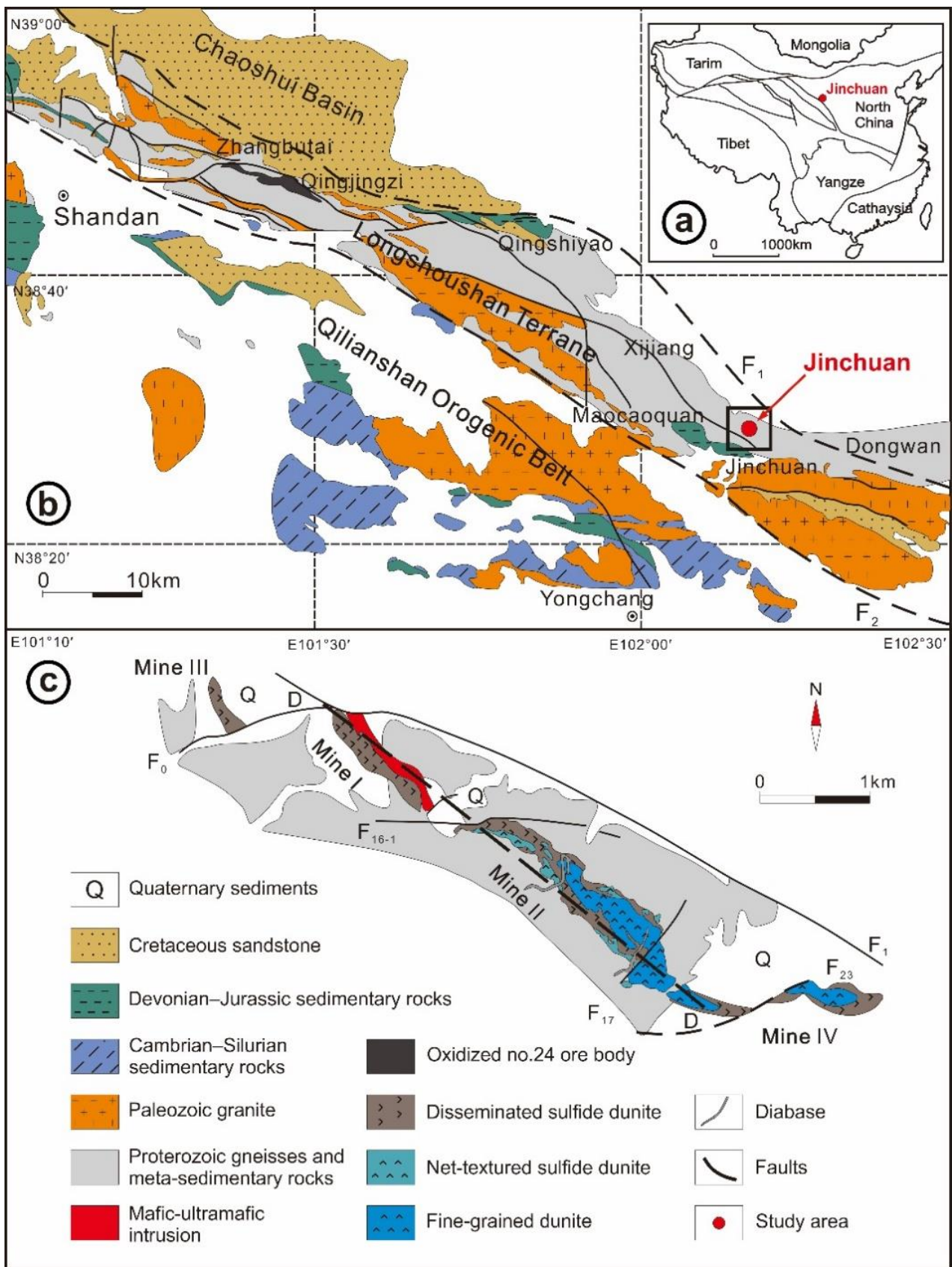


Figure 2. Simplified geological maps showing major tectonic units of China (a) (modified from [25]), location of the Jinchuan magmatic Ni-Cu ore deposit in the Longshoushan terrane in the context of regional geology (b) and distribution of ore bodies in the Jinchuan deposit (c) (modified from [26,27]).

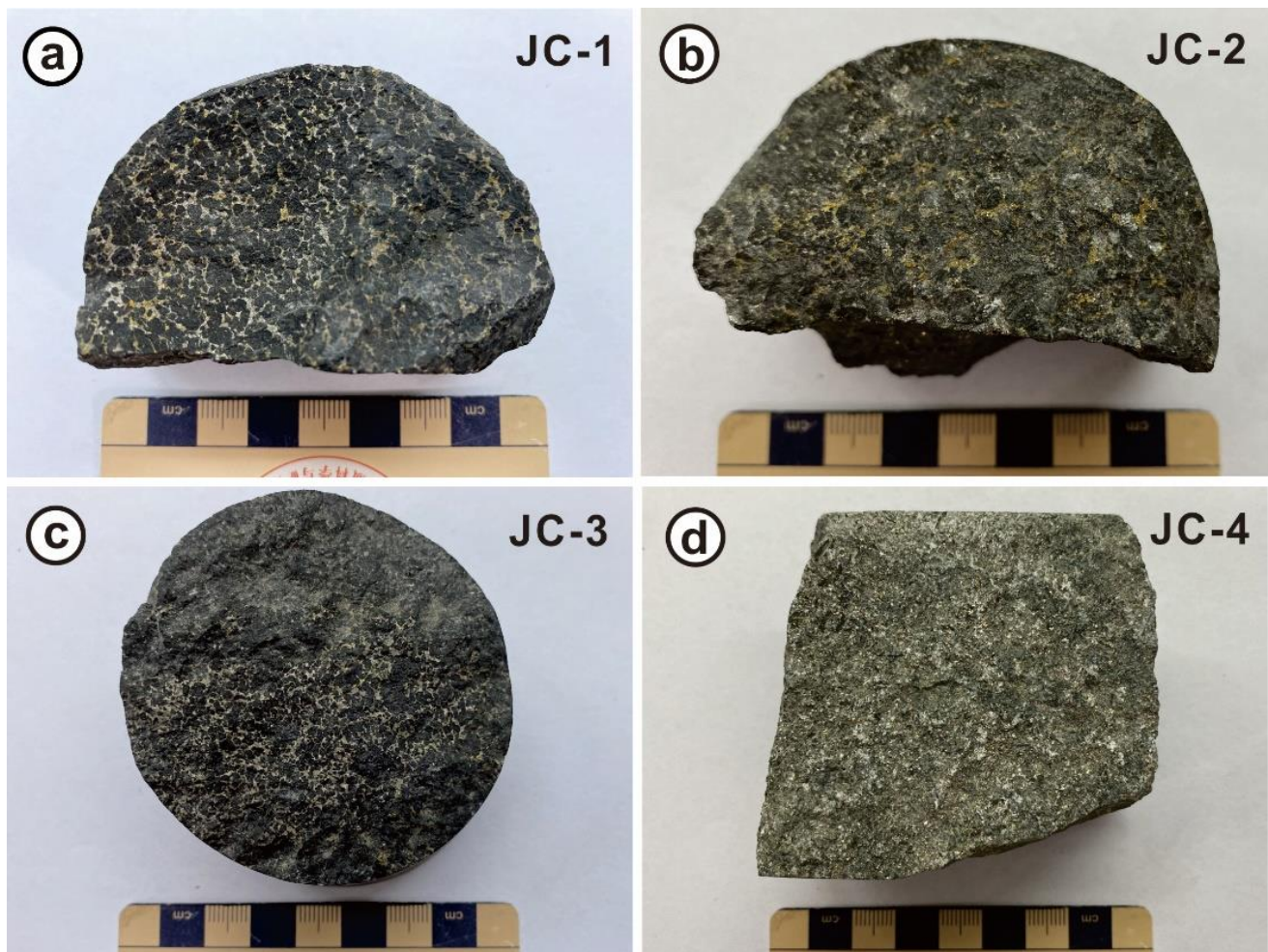


Figure 3. Photographs of the typical net-textured (a–c) and disseminated (d) sulfide ore samples from the Jinchuan Ni-Cu sulfide deposit. Samples JC-1, 2, and 3 are net-textured ores with sulfides filling the interstices between silicate mineral grains, sample JC-4 is a disseminated ore with sulfides sparsely dispersed between silicate mineral grains.

3. Sample and Methods

3.1. Sample

We collected four fresh drill core sulfide ore samples from the Jinchuan deposit (Figure 3). Samples JC-1, 2, and 3 were net-textured ores with sulfides filling the interstices between silicate mineral grains. JC-1 and JC-2 were sulfide-rich dunite dominated by olivine and sulfide, and JC-3 was sulfide-rich lherzolite dominated by olivine, pyroxene (orthopyroxene > clinopyroxene), and sulfide. Sample JC-4 was a disseminated ore with sulfides sparsely dispersed between silicate mineral grains, which was collected from the metasomatic orebody at the contact of the ultrabasic intrusion with dolomite marble, which was dominated by dolomite with a small amount of amphibole (tremolite and actinolite) and phlogopite. Silicate minerals dominated by olivine are partially or entirely serpentinized (Figure 4), with minor magmatic chromite (or chrome spinel) and secondary magnetite traces. The sulfide mineral assemblage in different ores was similar, dominated by pyrrhotite (~55% of all sulfides), pentlandite (~30%), and chalcopyrite (~15%). Minor cubanite can be found in some samples (less than 2%; Figure 4d,e). Serpentine was the most abundant altered mineral after olivine and pyroxene and takes the pseudomorphs of these silicate minerals without showing any deformation. Small olivine relicts were locally seen in mesh-textured serpentines. Except for sample JC-4, there were minor other altered minerals such as phlogopite, amphibole, and dolomite (less than 1% in net-textured ore samples JC-1, 2, and 3) (Figure 4d,i).

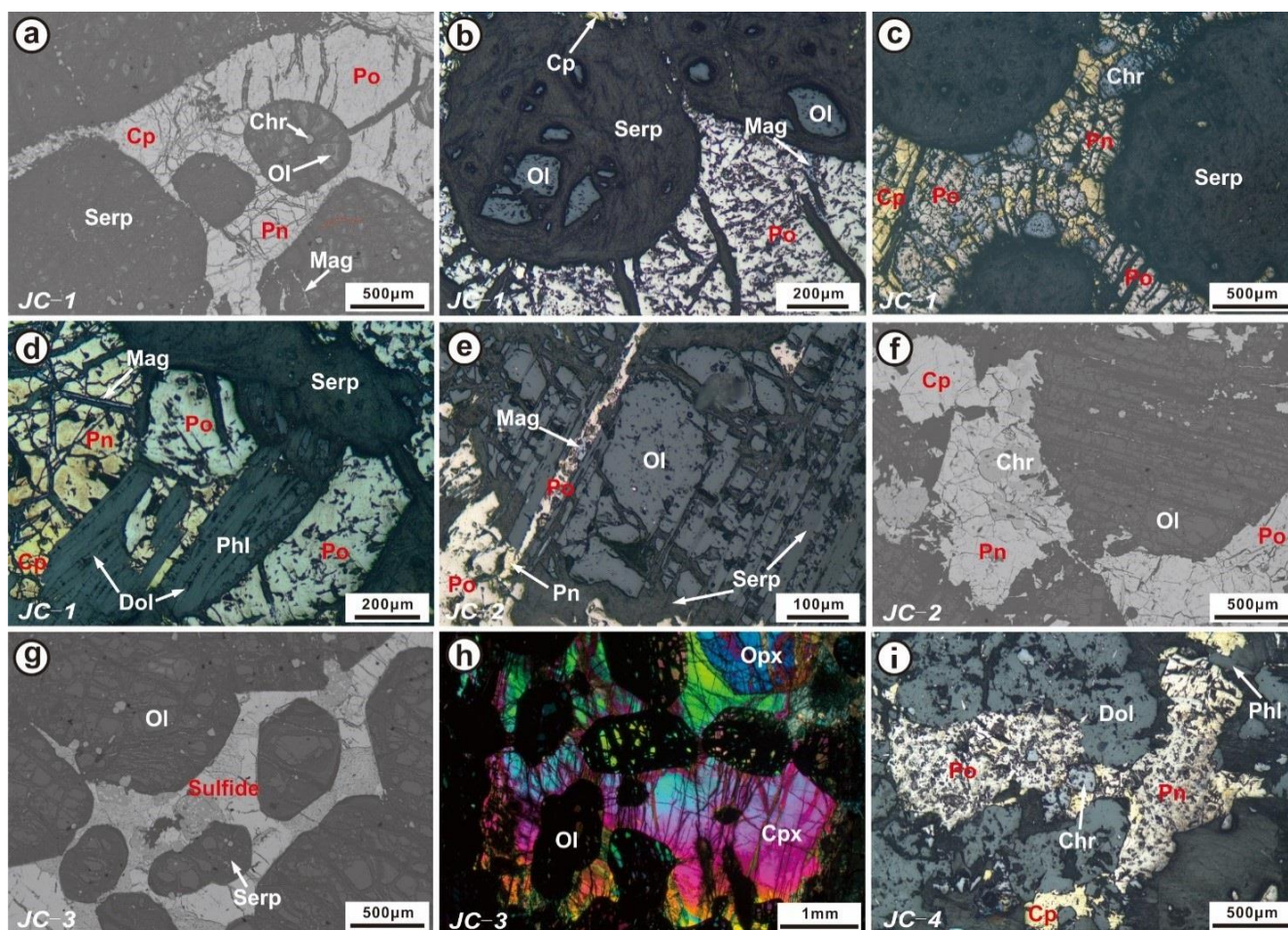


Figure 4. Photomicrographs and backscattered electron images of coexisting minerals from net-textured ores (JC-1 (a–d), JC-2 (e,f), and JC-3 (g,h)) and disseminated ore (JC-4 (i)) under transmitted light (h), reflected light (b–e,i). Panels of a and f–g are backscattered electron images. (a) Sample JC-1 is a net-textured sulfide-rich dunite, where olivine is almost entirely serpentinized with tiny olivine relicts preserved for analysis (Fo = 82–84%) and minute secondary magnetite traces along cracks. The sulfides are mostly pyrrhotite, pentlandite, and chalcopyrite. (b) Serpentine takes the pseudomorphs after euhedral olivine with minute relicts. Pyrrhotite accounts for half of all the sulfide minerals. (c) Similar to (a) and (b), but there are chromite granules coexisting with sulfide minerals as indicated. (d) Minor secondary magnetite of serpentinization origin along cracks and grain boundaries of sulfide minerals. There are also grains of dolomite and phlogopite formed by the late alteration. (e) Sample JC-2 is a net-textured sulfide-rich dunite with serpentinization occurring along the olivine cracks. (f) Sulfide minerals are connected to form a network between serpentinized olivine grains. (g) Sample JC-3 is a net-textured sulfide-rich lherzolite with minor serpentinization. (h) Fresh portion of JC-3, showing cumulate of olivine, orthopyroxene, and minor clinopyroxene. The clinopyroxene is anhedral as interstitial fills between olivine and orthopyroxene. (i) Sample JC-4 is a disseminated sulfide-rich altered ore from metasomatic orebody, containing altered dolomite, phlogopite, and amphibole with minor serpentine. Mineral abbreviations: Ol = olivine; Srp = serpentine; Cpx = clinopyroxene; Opx = orthopyroxene; Chr = chromite; Mag = magnetite; Po = pyrrhotite; Cp = chalcopyrite; Pn = pentlandite; Dol = dolomite; Phl = phlogopite.

Detailed petrography of these four ore samples is given in Table 1. Representative photomicrographs and backscattered electron images are shown in Figure 4. Samples JC-1 and 2 were sulfide-rich dunite having 70–80% olivine (highly serpentinized), sample JC-3 was a sulfide-rich lherzolite, consisting of olivine and pyroxenes (orthopyroxene > clinopyroxene), and sample JC-4 was a sulfide-rich altered ore, which was mainly composed of dolomite, phlogopite, amphibole, and minor serpentine.

Table 1. Petrography of studied ore samples from the Jinchuan deposit.

Sample No.	Ore Type	Petrographic Description
JC-1	Net-textured ore	sulfide-rich dunite, composed chiefly of olivine (~8%), which has been completely altered to serpentine (~68%) (olivine + serpentine ≈ 76%). The interstitial space between olivine grains is mainly filled by sulfides (~22%), including pyrrhotite (~12%), chalcopyrite (~4%), and pentlandite (~6%), forming the structure of spongy meteorite (net-texture), minor Cr-spinel (~1%) and altered minerals (~1%).
JC-2	Net-textured ore	sulfide-rich dunite, composed chiefly of olivine (~32%), which has been strongly serpentinized (~46%) (olivine + serpentine ≈ 78%). The interstitial space between olivine grains is mainly filled by sulfides (~18%), including pyrrhotite (~10%), chalcopyrite (~2%), and pentlandite (~6%), forming the structure of spongy meteorite (net-texture), minor Cr-spinel (~1%), and altered minerals (~3%).
JC-3	Net-textured ore	sulfide-rich lherzolite, consists of olivine (~50%), pyroxenes (~35%; orthopyroxene (~20%) > clinopyroxene (~15%)), plagioclase (~4%), and minor Cr-spinel (~1%). Metallic sulfides are mainly composed of pyrrhotite (~5%), chalcopyrite (~3%), pentlandite (~2%), and minor cubanite.
JC-4	Disseminated ore	sulfide-rich altered ore from metasomatic orebody at the contact of the mafic intrusion with dolomite marble dominated by dolomite (~50%), phlogopite (~16%), amphibole (~12%), sulfide (~16%), and a small amount of serpentine (~6%).

The mineral modes in each sample are determined by point-counting.

3.2. Methods

Four ore samples (JC-1–4) (Figure 3) were made thin sections and separated for minerals (i.e., pyrrhotite, chalcopyrite, pentlandite, serpentine, magnetite, olivine, clinopyroxene, and orthopyroxene) in the Hebei Geological Survey. Major element analysis on sulfides were done using a JXI-8100 Electron Microprobe Analyser (EMPA) in the Key Lab of Mineral Resources and Geological Engineering, Chang'an University in China. The analytical conditions were 15 kV voltage, 1.0×10^{-8} A electric current, and 1 μm beam spot. The analytical data on sulfides are given in Table 2.

Major and trace element analyses on silicate and oxide minerals were done using laser ablation inductively coupled plasma mass spectrometer (LA-ICP-MS) in the Laboratory of Ocean Lithosphere and Mantle Dynamics, Institute of Oceanology, Chinese Academy of Sciences (IOCAS). The instrument consists of a 193 nm excimer Ar-F laser ablation system attached to an Agilent-7900 inductively coupled plasma mass spectrometer. The analytical conditions were 40 μm ablation beam spot, 3.94 J/cm² energy density, and 6 Hz frequency. Each analysis included 25 s background collection (gas blank) and 50 s data collection. United States Geological Survey (USGS) rock standards (BHVO-2G, BIR-1G, and BCR-2G) were used as external standards for calibration, and Si was used to correct for instrumental drift following [39]. The raw data were processed using ICPMSDataCal_ver11.0 [39,40] and data quality was assessed by repeated analyses of GSE-1G over the analytical session. The analytical data on silicate and oxide minerals are given in Table 3.

The major and trace element analyses of the bulk-rock ore samples and mineral separates were done in the Laboratory of Ocean Lithosphere and Mantle Dynamics, IOCAS. The bulk-rock samples were digested using the alkali dissolution method, while mineral separates were digested using the acid dissolution method. The major elements of the samples were analyzed using an inductively coupled plasma optical emission spectrometer (ICP-OES, i.e., an Agilent-5100) with USGS rock standards (BCR-2 and BHVO-2) used to monitor the data quality following [41]. The analytical error of major elements is <5%. However, as alkali dissolution causes S loss in bulk-rock ore samples and the acid dissolution causes S and Si losses in mineral separates, these elements were thus unanalyzed.

Given the small sample size, no loss-on-ignition was done. Therefore, the totals of major elements of bulk-rock ore samples and mineral separates were variably less than 100%, but this did not compromise our research objective. The trace elements of the samples were measured using an inductively coupled plasma mass spectrometer (ICP-MS, i.e., an Agilent-7900) with the data quality better than 10%, following the method detailed in [42]. The analytical data are given in Table 4.

Table 2. Averaged major element content of each sulfide mineral of ore samples in the Jinchuan deposit by EMPA analysis.

Sample No.	Ore Type	Sulfide Mineral	Calculated Molecular Formula	N	S	Fe	Cu	Ni	Total
					wt.%	wt.%	wt.%	wt.%	wt.%
JC-1	Net-textured ore	Pyrrhotite	Fe _{0.855} S	36	39.86	59.37	0.044	0.092	99.53
		Chalcopyrite	Cu _{0.944} Fe _{0.959} S ₂	32	36.20	30.23	33.85	0.051	100.5
		Pentlandite	(Fe _{4.531} ,Ni _{3.825}) _{8.355} S ₈	25	34.51	34.04	0.051	30.20	99.31
JC-2	Net-textured ore	Pyrrhotite	Fe _{0.852} S	26	40.42	60.01	0.052	0.202	100.8
		Chalcopyrite	Cu _{0.912} Fe _{0.930} S ₂	13	36.62	29.65	33.09	0.018	99.57
		Pentlandite	(Fe _{4.125} ,Ni _{4.038}) _{8.164} S ₈	22	34.15	30.67	0.087	31.56	97.31
JC-3	Net-textured ore	Pyrrhotite	Fe _{0.889} S	15	39.74	61.53	0.059	0.044	101.5
		Chalcopyrite	Cu _{0.885} Fe _{0.948} S ₂	18	36.79	30.36	32.27	0.011	99.60
		Pentlandite	(Fe _{4.026} ,Ni _{3.507}) _{7.533} S ₈	13	36.31	31.83	0.249	29.14	98.35
		Cubanite	Cu _{0.857} Fe _{1.849} S ₃	5	37.94	40.71	21.47	0.022	100.3
JC-4	Disseminated ore	Pyrrhotite	Fe _{0.826} S	13	41.38	59.51	0.051	0.492	101.6
		Chalcopyrite	Cu _{0.897} Fe _{0.937} S ₂	8	36.95	30.16	32.85	0.081	100.3
		Pentlandite	(Fe _{3.997} ,Ni _{3.930}) _{7.928} S ₈	12	35.45	30.85	0.064	31.88	99.00

N = number of grains analyzed.

Iron isotope compositions of mineral separates from the four sulfide ore samples were measured in the Laboratory of Ocean Lithosphere and Mantle Dynamics, IOCAS. Mineral separates were cleaned ultrasonically in Milli-Q water before digestion in HF-HNO₃-HCl on a hotplate. After repeated reflux using reverse aqua regia to obtain full digestion, the samples were finally dissolved in 1 mL of 9 N HCl and ready for chromatographic separation for Fe. Fe was purified using 1 mL of anion exchange resin (Bio-Rad AG MP-1M 200 400 mesh) conditioned with 9 N HCl, following the procedure of [43]. Matrix elements including Ni and Cr were removed by washing with 5 mL of 9 N HCl. The columns were then washed with 5 mL of 6 N HCl to remove Cu and possible residual Cr and Ni. Fe was eluted from columns by using 2 mL of 1 N HCl. The eluted Fe solutions were analyzed using ICP-OES to ensure purity and full recovery. The total procedural blank for Fe was 80 ng, which was less than 0.01% of the processed samples and was thus negligible. Prior to measurements, Fe solutions were diluted to 7 ppm, and 9.8 ppm GSB Ni standard (an ultrapure single elemental standard solution from the China Iron and Steel Research Institute) was added as an internal mass bias monitor to each diluted sample (Ni:Fe = 1.4:1). Iron isotope compositions of mineral separates were analyzed using a Nu plasma multi-collector inductively coupled plasma mass spectrometer (MC-ICP-MS) with wet nebulization. Backgrounds were measured and subtracted using electrostatic analyzer (ESA) deflection. Contributions from isobaric interferences (⁴⁰Ar¹⁴N on ⁵⁴Fe and ⁴⁰Ar¹⁶O on ⁵⁶Fe) were eliminated by measuring in pseudo-high resolution mode with M/DM of >8000. The mass bias fractionation during analysis was corrected for using the Ni doping method (⁶⁰Ni/⁵⁸Ni) with ⁵⁸Fe interference on ⁵⁸Ni corrected based on ⁵⁶Fe [44–46]. The iron isotope data are expressed using the standard notation $\delta^{56}\text{Fe} = \left[\frac{(^{56}\text{Fe}/^{54}\text{Fe})_{\text{sample}}}{(^{56}\text{Fe}/^{54}\text{Fe})_{\text{IRMM-014}}} - 1 \right] \times 1000$. During analysis, every five sample solutions were bracketed with 7 ppm GSB Fe standard solution that was also doped with the GSB Ni solution with Ni:Fe of 1.4:1 (the Fe isotope composition of GSB Fe relative to IRMM-014 is $\delta^{57}\text{Fe}_{\text{IRMM-014}} = \delta^{57}\text{Fe}_{\text{GSB}} + 1.073$ and $\delta^{56}\text{Fe}_{\text{IRMM-014}} = \delta^{56}\text{Fe}_{\text{GSB}} + 0.729$ [47]). Every sample solution was repeatedly analyzed four times, with the average $\delta^{57}\text{Fe}$ and $\delta^{56}\text{Fe}$ values of each sample given in Table 5. Long-term analyses of an in-house Alfa Fe standard (an ultrapure single elemental standard from the Alfa Aesar Chemicals Co., Ltd.) given an average $\delta^{56}\text{Fe}$ value of $0.51 \pm 0.05\text{‰}$ (2SD, $n = 37$). The $\delta^{56}\text{Fe}$ value of the USGS standard BCR-2 analyzed together with our samples was $0.13 \pm 0.03\text{‰}$ (2SD, $n = 10$), consistent with the recommended literature value [47,48]. Duplicate digestion, chemical separation and analyses of two samples (JC-4 Pentlandite and JC-4 Pentlandite-R) show good reproducibility (Table 5). Analytical details are given in [43].

Table 3. Representative microprobe analyses of silicate and oxide minerals of ore samples in the Jinchuan deposit by LA-ICP-MS.

Sample No.	Standard			JC-1			JC-2			JC-3				JC-4			
	Mineral	BIR-1G	BCR-2G	BHVO-2G	Olivine	Serpentine	Chromite	Olivine	Serpentine	Chromite	Olivine	Serpentine	Chromite	Clinopyroxene	Orthopyroxene	Plagioclase	Serpentine
N	24	24	24	4	3	12	4	4	9	3	3	7	4	4	2	8	
Major elements (wt.%)																	
SiO ₂	46.84	53.02	49.01	38.19	36.12	0.052	38.80	38.75	0.081	38.54	38.71	0.058	50.18	53.69	53.38	39.97	
TiO ₂	0.929	2.254	2.698	0.017	0.434	0.925	0.012	0.020	1.471	0.021	0.012	1.150	0.417	0.195	0.106	0.020	
Al ₂ O ₃	15.23	13.91	14.28	0.023	3.842	9.636	0.026	2.623	0.133	0.041	0.028	15.69	3.630	2.186	29.25	0.038	
FeO _T	11.52	13.91	11.79	15.43	9.003	51.64	16.52	7.738	75.96	16.72	13.24	39.22	5.812	9.496	0.418	14.68	
MnO	0.178	0.205	0.173	0.203	0.712	0.389	0.303	0.086	0.394	0.229	0.251	0.322	0.155	0.206	0.004	0.052	
MgO	9.371	3.501	7.011	45.17	34.93	3.163	43.22	37.01	0.630	43.57	33.14	4.938	18.84	30.94	0.130	31.25	
CaO	13.12	7.108	11.33	0.141	0.042	0.033	0.387	0.009	0.014	0.126	0.371	0.014	19.27	2.220	11.47	0.164	
Na ₂ O	1.862	3.218	2.284	0.006	0.018	0.068	0.026	0.004	0.003	0.027	0.123	0.298	0.049	4.804	0.059	0.059	
K ₂ O	0.021	1.748	0.522	-	0.009	0.017	0.014	0.004	0.027	0.001	0.014	0.021	-	0.001	0.279	0.032	
P ₂ O ₅	0.051	0.356	0.278	0.038	0.019	0.030	0.037	0.016	0.035	0.044	0.040	0.019	0.024	0.029	0.038	0.038	
Cr ₂ O ₃	0.057	0.002	0.042	0.014	1.501	32.15	0.012	0.425	13.10	0.017	0.010	37.64	1.107	0.625	-	0.055	
NiO	0.022	0.001	0.015	0.304	0.042	0.087	0.144	0.073	0.372	0.186	0.292	0.080	0.030	0.048	0.001	0.177	
FeO _{cal.}	-	-	-	-	-	28.96	-	-	30.46	-	-	27.82	-	-	-	-	
Fe ₂ O ₃ cal.	-	-	-	-	-	25.21	-	-	50.56	-	-	12.67	-	-	-	-	
Total	99.30	99.36	99.52	99.53	86.73	100.7	99.51	86.77	97.40	99.49	86.14	100.6	99.81	99.71	99.88	86.55	
Trace element (ppm)																	
Li	2.922	8.934	4.573	2.745	8.089	0.463	7.076	1.434	8.287	5.396	0.184	0.622	17.08	2.492	0.205	7.453	
Be	0.142	2.728	1.364	0.172	0.094	-	0.136	0.103	0.283	0.018	0.129	0.100	0.025	0.038	0.612	0.063	
Sc	42.67	33.56	32.31	4.523	72.00	1.380	2.943	13.54	1.326	5.595	4.782	1.088	64.81	29.16	0.397	18.84	
V	534.2	704.2	441.9	3.093	291.1	9844	2.679	39.46	1096	6.076	6.303	1871	275.3	120.9	2.742	7.568	
Cr	388.4	15.14	286.5	97.83	10272	-	79.66	2910	-	115.7	71.10	-	7574	4273	2.000	378.8	
Co	53.24	37.83	45.37	139.0	27.29	180.2	78.73	28.13	66.72	176.8	156.2	494.7	40.74	74.99	0.228	97.86	
Ni	172.5	11.64	117.5	2387	329.7	683.6	1129	571.0	2919	1459	2291	630.6	233.3	375.7	8.157	1395	
Cu	120.8	16.67	129.1	0.089	2.106	14.00	0.766	0.137	0.030	0.030	470.6	0.028	0.830	0.279	0.355	71.54	
Zn	74.37	139.1	105.5	120.9	8.064	1577	98.60	33.43	664.8	109.1	17.14	3365	29.54	73.53	2.479	59.12	
Ga	15.60	21.75	21.48	0.086	3.610	36.42	0.064	4.939	11.72	0.228	2.122	78.84	5.732	4.073	25.37	0.706	
Ge	1.132	2.363	2.763	5.037	1.300	-	5.450	1.616	1.138	1.551	2.300	0.559	3.041	11.15	2.453	2.828	
Rb	0.271	46.39	9.373	0.015	0.211	-	1.013	1.548	-	0.067	0.094	-	0.033	0.146	1.002	3.842	
Sr	106.8	341.7	391.0	0.014	0.624	1.879	2.044	0.228	0.804	0.188	4.305	0.006	19.27	0.506	671.9	38.59	
Y	15.03	35.72	25.49	0.319	10.69	0.026	0.562	0.538	-	0.454	0.686	0.005	12.31	2.121	0.401	4.087	
Zr	13.79	182.8	165.9	0.109	11.43	0.144	0.254	0.384	-	0.258	0.527	0.950	12.13	1.807	0.112	0.193	
Nb	0.511	13.49	20.40	0.003	0.058	0.040	0.230	0.223	0.066	0.001	0.011	0.098	0.023	0.005	0.015	0.415	
Mo	0.045	237.1	3.727	0.043	0.450	0.322	0.066	0.632	0.069	0.022	0.038	0.068	0.067	0.016	0.030	7.022	
Cs	0.016	1.310	0.161	0.032	0.041	-	0.237	0.364	-	0.017	0.015	-	0.014	0.023	0.032	1.060	
Ba	6.594	687.4	128.7	0.021	2.643	1.605	7.628	2.537	0.809	0.107	2.652	-	0.150	0.395	233.1	12.27	
La	0.581	25.08	14.89	0.346	1.185	0.058	0.089	0.106	0.005	0.005	0.160	-	0.807	0.009	3.481	0.387	
Ce	1.810	53.02	36.73	0.002	4.515	0.084	0.267	0.238	0.037	0.008	0.353	-	3.502	0.074	6.194	1.259	
Pr	0.366	6.737	5.139	0.001	0.760	0.006	0.046	0.029	0.005	0.001	0.049	-	0.709	0.013	0.617	0.213	
Nd	2.360	28.56	24.09	0.029	4.182	-	0.191	0.190	0.038	0.004	0.170	-	4.462	0.137	2.300	1.125	
Sm	1.047	6.494	6.031	0.033	1.329	0.025	0.064	0.063	-	0.003	0.024	-	1.742	0.074	0.304	0.399	
Eu	0.520	2.061	2.284	0.004	0.472	-	0.018	0.025	0.035	0.002	0.007	-	0.517	0.034	1.039	0.126	
Gd	1.769	6.814	6.044	0.014	1.959	0.012	0.075	0.060	0.085	0.009	0.022	-	2.186	0.174	0.299	0.502	
Tb	0.360	1.161	1.083	0.004	0.308	-	0.013	0.007	0.008	0.002	0.007	-	0.352	0.038	0.027	0.090	
Dy	2.722	7.779	7.546	0.067	2.102	0.015	0.116	0.105	0.034	0.037	0.061	0.009	2.374	0.287	0.106	0.650	
Ho	0.580	1.470	1.186	0.016	0.432	0.002	0.028	0.017	0.016	0.014	0.016	-	0.476	0.076	0.019	0.166	
Er	1.644	3.617	2.520	0.041	1.220	0.016	0.063	0.085	-	0.070	0.104	-	1.327	0.288	0.029	0.578	
Tm	0.237	0.522	0.318	0.012	0.168	0.003	0.019	0.016	-	0.014	0.030	0.002	0.188	0.047	0.007	0.103	
Yb	1.596	3.373	2.003	0.111	1.063	-	0.125	0.089	0.050	0.139	0.235	0.040	1.171	0.362	0.006	0.711	
Lu	1.778	7.392	5.266	0.011	0.155	-	0.015	0.021	0.009	0.026	0.055	0.002	0.158	0.057	0.003	0.158	
Hf	1.545	21.03	25.84	0.013	0.557	0.020	0.019	0.016	0.013	0.004	0.011	0.013	0.584	0.089	0.019	0.004	
Ta	0.027	0.790	1.166	0.004	0.004	-	0.012	0.008	0.003	-	0.002	-	0.007	0.001	0.006	0.022	
Pb	3.535	10.74	1.799	0.045	0.255	0.247	16.17	3.347	18.01	0.035	4.078	-	0.226	0.063	0.693	4.215	
Th	0.032	11.56	2.819	0.004	0.021	0.005	0.018	0.048	0.010	-	0.002	-	0.012	0.002	0.005	0.112	
U	0.015	1.653	0.412	0.002	0.011	-	0.035	0.083	0.043	0.001	0.003	-	0.005	0.003	0.011	0.216	

N = number of grains analyzed. The “-” indicates that element content is below the detection limit.

Table 4. Major and trace element compositions of bulk-rock ore samples and mineral separates in Jinchuan deposit by ICP-OES and ICP-MS, respectively.

Sample No.	Bulk-Rock Ores/Mineral Separates	Major Elements (wt.%, ICP-OES)													
		SiO ₂	TiO ₂	Al ₂ O ₃	FeO _T	MnO	MgO	CaO	Na ₂ O	K ₂ O	P ₂ O ₅	CuO	NiO	Cr ₂ O ₃	Total
bulk-rock ores (Alkali dissolution)	BLANK	0.019	-	-	0.001	-	0.001	0.027	0.002	0.001	0.007	-	-	-	0.058
Standard	BCR-2	55.44	2.265	13.12	12.21	0.196	3.603	7.092	3.175	1.841	0.385	0.002	0.002	0.003	99.34
	BHVO-2	50.43	2.728	13.10	10.84	0.166	7.205	11.27	2.167	0.499	0.284	0.014	0.017	0.040	98.76
Whole ore	JC-1	24.89	0.062	0.626	24.49	0.126	25.20	0.411	0.039	0.061	-	2.682	2.500	0.501	81.59
	JC-2	25.41	0.065	1.003	26.07	0.148	24.40	1.505	0.025	0.030	-	1.135	4.013	0.464	84.27
	JC-3	36.43	0.337	2.355	16.49	0.179	27.73	2.132	0.224	0.273	0.032	1.220	0.971	0.469	88.85
	JC-4	25.76	0.078	0.634	22.06	0.199	19.34	6.429	0.048	0.231	0.024	0.475	2.954	0.646	78.88
Replicate samples	JC-3-R	36.71	0.342	2.385	16.48	0.181	27.77	2.121	0.238	0.305	0.035	1.245	0.972	0.491	89.28
Silicate/oxide mineral separates (Acid dissolution)		SiO ₂	TiO ₂	Al ₂ O ₃	FeO _T	MnO	MgO	CaO	Na ₂ O	K ₂ O	P ₂ O ₅	CuO	NiO	Cr ₂ O ₃	Total
JC-1	Serpentine	-	0.211	0.660	5.408	0.062	14.45	0.134	0.034	0.006	0.005	0.029	0.051	0.583	21.63
	Magnetite	-	0.911	8.449	64.00	0.564	2.704	0.094	0.006	0.013	-	0.063	0.127	23.92	100.9
JC-2	Serpentine	-	0.050	2.310	9.460	0.095	27.39	0.144	0.007	0.002	0.007	0.027	0.073	0.373	39.94
	Magnetite	-	1.321	0.211	87.48	0.421	1.652	0.079	0.014	0.019	0.001	0.040	0.159	8.622	100.0
JC-3	Olivine	-	0.035	0.145	16.15	0.226	38.57	0.328	0.008	0.002	0.013	0.002	0.183	0.080	55.74
	Clinopyroxene	-	0.537	3.789	6.274	0.167	19.37	19.51	0.346	0.027	-	0.004	0.029	0.968	51.02
JC-4	Orthopyroxene	-	0.274	2.434	10.30	0.221	31.48	2.817	0.060	0.011	0.010	0.004	0.050	0.590	48.25
	Magnetite	-	0.955	0.151	81.57	0.236	0.676	0.579	0.005	-	-	0.057	0.147	8.239	92.62
Replicate samples	JC-4 Magnetite-R	-	0.955	0.148	82.03	0.236	0.679	0.536	0.004	0.001	0.002	0.062	0.158	9.016	93.83
Sulfide mineral separates (Acid dissolution)		Si	Ti	Al	Fe	Mn	Mg	Ca	Na	K	P	Cu	Ni	Cr	Total
JC-1	Pyrrhotite (+Pentlandite)	-	0.008	0.064	47.73	0.050	3.307	0.910	0.006	0.027	0.041	1.674	11.26	0.066	65.15
	Chalcopyrite (+Pentlandite)	-	0.008	0.029	37.87	0.012	0.586	0.373	0.001	0.041	0.332	18.73	15.52	0.004	73.50
	Pentlandite	-	0.005	0.015	36.07	0.004	0.327	0.216	0.015	0.037	0.003	0.228	30.50	0.009	67.42
JC-2	Pyrrhotite (+Pentlandite)	-	0.003	0.039	48.12	0.016	1.710	0.085	-	0.025	0.009	0.383	16.53	0.008	66.92
	Chalcopyrite	-	0.001	0.025	31.93	0.012	0.878	0.100	-	0.024	0.384	29.74	1.445	0.002	64.53
JC-3	Pentlandite	-	0.003	0.007	34.02	0.004	0.483	0.041	-	0.018	0.008	0.680	34.92	0.002	70.18
	Pyrrhotite	-	5.281	2.522	55.94	0.272	1.480	5.760	0.031	0.017	-	0.172	0.096	5.978	77.55
JC-4	Pyrrhotite (+Pentlandite)	-	0.002	0.012	59.24	0.002	0.225	0.091	-	-	0.003	0.526	6.114	0.010	66.22
	Pentlandite	-	0.004	0.012	33.40	0.002	0.260	0.323	-	0.017	0.017	0.761	35.16	0.003	69.96
Replicate samples	JC-4 Pentlandite-R	-	0.004	0.008	33.33	0.002	0.250	0.055	-	0.014	0.013	0.693	34.57	0.003	68.94

The “-” indicates that element content is below the detection limit. Pyrrhotite (+pentlandite) = pyrrhotite separate mixed with pentlandite.

Table 5. The iron isotope compositions of sulfide, silicate, and oxide mineral separates of ore samples in the Jinchuan deposit analyzed by MC-ICP-MS.

Sample No.	Mineral Separates	$\delta^{56}\text{Fe}$ (‰)	2SD	$\delta^{57}\text{Fe}$ (‰)	2SD
Standard	BCR-2	0.13	0.03	0.11	0.04
	BHVO-2	0.11	0.02	0.03	0.05
	AGV-2	0.12	0.07	0.07	0.04
	W-2a	0.02	0.02	0.03	0.07
JC-1	Pyrrhotite (+Pentlandite)	−0.82	0.04	−1.19	0.09
	Chalcopyrite (+Pentlandite)	0.15	0.06	0.17	0.11
	Pentlandite	0.53	0.03	0.86	0.04
	Serpentine	0.60	0.05	0.88	0.05
	Magnetite	0.24	0.04	0.38	0.03
JC-2	Pyrrhotite (+Pentlandite)	−0.16	0.01	−0.26	0.05
	Chalcopyrite	0.50	0.04	0.65	0.06
	Pentlandite	1.05	0.05	1.60	0.10
	Serpentine	0.52	0.02	0.60	0.05
	Magnetite	0.71	0.05	1.07	0.06
JC-3	Pyrrhotite	−0.77	0.05	−1.17	0.07
	Olivine	0.07	0.03	0.11	0.09
	Clinopyroxene	0.04	0.02	−0.02	0.04
	Orthopyroxene	0.05	0.07	0.03	0.09
JC-4	Pyrrhotite (+Pentlandite)	−0.90	0.03	−1.33	0.05
	Pentlandite	1.02	0.04	1.57	0.04
	Magnetite	0.50	0.03	0.79	0.06
Replicate samples	JC-4 Pentlandite-R	0.99	0.03	1.46	0.06
	JC-4 Magnetite-R	0.44	0.04	0.75	0.02

2SD = two times the standard deviation of the population of repeated measurements of a sample solution. Pyrrhotite (+pentlandite) = pyrrhotite separate mixed with pentlandite.

4. Results

4.1. Mineral Chemistry

Table 2 gives the in situ analyses using EMPA and Table 3 gives the in situ analyses using LA-ICP-MS on ore minerals (sulfide) and gangue minerals (silicate, oxide, etc.). On the basis of the major element analyses, chemical formula of the mean composition for each mineral was calculated and given in Table 2. The calculations were done using the combined method of stoichiometry and charge balance considerations. For serpentine, the calculation assumed the anion as $\text{O}_{10}(\text{OH})_8$. The olivine composition was relatively uniform with $\text{Fo} = 0.82\text{--}0.84$. Serpentine contains 7.74–14.68 wt.% of FeO, suggesting that iron from olivine remain largely retained during serpentinization.

4.2. Bulk-Rock Ore Sample Major Element Composition

The major element compositions of bulk-rock ore samples are given in Table 4, which were used for calculating chemical formulae of varying minerals.

4.3. Iron Isotopes of Mineral Separates

Mineral separates were analyzed for iron isotope composition to examine possible iron isotope fractionation between coexisting minerals. The major challenge is to obtain pure minerals from fine-grained and intertwined mineral aggregates in ore samples. Mineral separation was done using the combined method of mechanical, magnetic, and heavy

liquid separation before the painstaking selection under a binocular. These led to sufficient purity for most mineral separates (all the silicate minerals, oxides and most sulfide minerals) as indicated by the mineral compositional analysis (Table 4). Only a few sulfide mineral separates may be less pure (e.g., pyrrhotite in JC-1,2,4, and chalcopyrite in JC-1,2, marked with “mineral separate (+mixed mineral)” in Table 4) because they were intertwined fine-grained aggregates (Figure 4).

The major element compositions and calculated formulae (Table 2) indicate that there were predominantly three sulfide minerals (pyrrhotite, chalcopyrite, and pentlandite). Pyrrhotite contained only Fe and S, chalcopyrite contained only Cu, Fe, and S, and pentlandite contained only Ni, Fe, and S. Due to the relatively simple compositions of sulfides in ore samples, the excess Ni in pyrrhotite and chalcopyrite might suggest limited solid solutions or probably come from pentlandite impurities. The excess Cu in pentlandite might suggest limited solid solution or come from chalcopyrite impurities. Therefore, the content of each sulfide mineral in the impure sulfide mineral separate (i.e., mixture of these three sulfide minerals) could be readily calculated following the steps detailed in Appendix A using the major elemental compositions of mineral separates (Table 4) and the empirical molecular formulae of sulfides (Table 2).

The calculated results of each sulfide content in the impure mineral separates are given in Column A₂ of Table 6. We can obtain iron isotope composition of each pure sulfide end-member through further calculations. Previous studies suggested the iron isotope composition of bulk-rock ($\delta^{56}\text{Fe}$) can be calculated by using the iron isotope composition of each iron-bearing mineral ($\delta^{56}\text{Fe}_i$) and the mass fraction of iron of that mineral (C_i) in the total iron of the bulk-rock (Equation (1) [49]), where k represents the total amount of coexisting iron-bearing minerals in the bulk-rock. The simulated $\delta^{56}\text{Fe}$ values of the bulk-rock calculated using this formula were essentially consistent with the measured $\delta^{56}\text{Fe}$ values of the bulk-rock powder within analytical error according to previous works [49,50]. Thus, iron isotope compositions of pure sulfide end-members ($\delta^{56}\text{Fe}_i$; Table 6) can be calculated by assuming that impure sulfide mineral separates are the “bulk-rock” ($\delta^{56}\text{Fe}$) and various pure sulfide end-members are “constituent minerals” ($\delta^{56}\text{Fe}_i$) (see Appendix B for details).

$$\delta^{56}\text{Fe}_{\text{bulk-rock}} = \sum_{n=1}^k C_i \times \delta^{56}\text{Fe}_i \quad (1)$$

The iron isotope compositions of all the mineral separates from the Jinchuan sulfide ores varied significantly (Table 5) with all the data points plotting on the mass fractionation line (Figure 5a). As seen in the covariation of $\delta^{56}\text{Fe}$ with Fe of different minerals (Figure 5c), the $\delta^{56}\text{Fe}$ values of the same minerals were rather similar, well separated from other minerals, and did not depend on iron content. Sulfide minerals and magnetite from the disseminated ore (JC-4; from metasomatic orebody) were analyzed, and iron isotope compositions of these minerals in sample JC-4 were within the range of the other three net-textured ores (JC-1, 2, and 3; from ore-bearing cumulates). Thus, we did not treat these sulfide minerals and magnetite in JC-4 specifically or explain them separately.

Table 6. Calculation of iron isotope composition of pure sulfide end-members in net-textured sulfide ore samples.

Part 1. Mineral Separates.									
Sample No.	Mineral Separates	$\delta^{56}\text{Fe}$ (Mineral Separate)	$A_2 = \text{Sulfide Content of Mineral Separate (wt.\%)}$			$A_3 = \text{Fe Content of Mineral Separate}$	Value of C_i		
		(%, from Table 5)	Pyrrhotite	Chalcopyrite	Pentlandite	(wt.%, from Table 4)	C(Pyrrhotite)	C(Chalcopyrite)	C(Pentlandite)
JC-1	Pyrrhotite (+Pentlandite)	−0.82	57.3	5.1	37.6	47.73	70.3	3.2	26.5
	Chalcopyrite (+Pentlandite)	0.15	5.4	49.4	45.2	37.87	9.6	44.5	45.8
	Pentlandite	0.53	-	-	~100.0	36.07	-	-	~100.0
JC-2	Pyrrhotite (+Pentlandite)	−0.16	51.2	-	48.8	48.11	67.3	-	32.7
	Chalcopyrite	0.50	6.5	89.1	4.4	31.93	6.5	89.0	4.6
	Pentlandite	1.05	-	-	~100.0	34.02	-	-	~100.0
JC-3	Pyrrhotite	−0.77	~100.0	-	-	56.79	~100.0	-	-
JC-4	Pyrrhotite (+Pentlandite)	−0.90	82.6	-	17.4	59.23	90.2	-	9.8
	Pentlandite	1.02	-	-	~100.0	33.40	-	-	~100.0
Part 2. Pure Sulfide End-Members after Calculation.									
Sample No.	Sulfide Type	$A_1 = \text{Fe Content of Each Sulfide}$			$\delta^{56}\text{Fe}_i$				
		(wt.%, from Table 2)				%			
JC-1	Pyrrhotite	59.37			−1.37				
	Chalcopyrite	30.23			0.09				
	Pentlandite	34.04			0.53				
JC-2	Pyrrhotite	60.01			−0.74				
	Chalcopyrite	29.65			0.56				
	Pentlandite	30.67			1.05				
JC-3	Pyrrhotite	61.53			−0.77				
JC-4	Pyrrhotite	59.51			−1.11				
	Pentlandite	30.85			1.02				

The “-” indicates that mineral content is below 1%. $\delta^{56}\text{Fe}$ (impure mineral separate) = $\sum C_i \times \delta^{56}\text{Fe}_i$ (i = each pure mineral); $C_i = A_1 \times A_2 / A_3$.

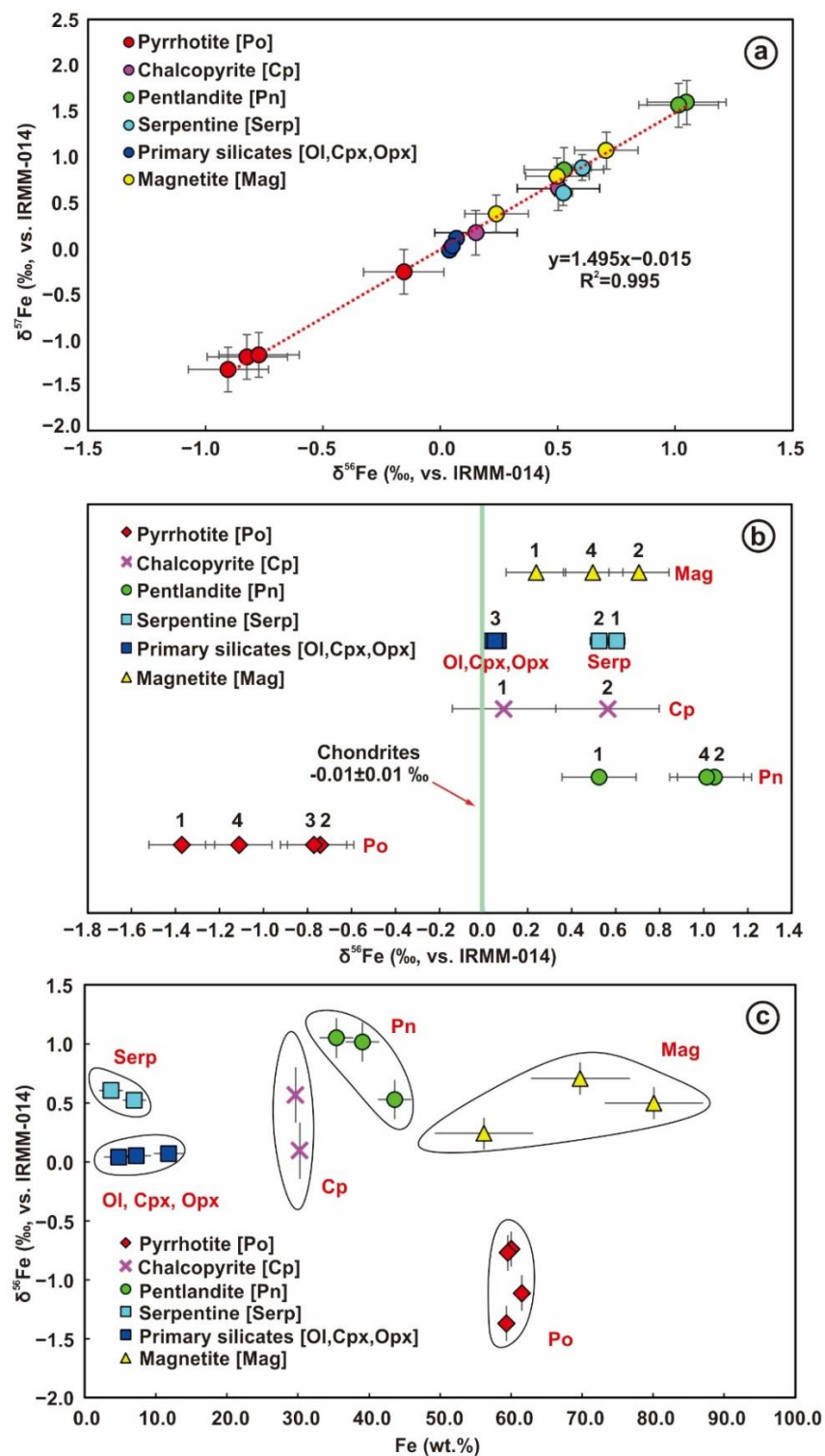


Figure 5. (a) Iron isotope compositions of the mineral separates from the Jinchuan sulfide ore samples plot along a mass-dependent fractionation line, confirming high quality of the data. Error bars represent ± 1 sd. (b) Iron isotope compositions of the mineral separates in ore samples from the Jinchuan deposit, compared with the carbonaceous chondrite data ($\delta^{56}\text{Fe} = -0.01 \pm 0.01$ ‰ ($n = 10$)) [2–6]. Numerals 1, 2, 3, and 4 represent samples JC-1, JC-2, JC-3, and JC-4. (c) The relationship between $\delta^{56}\text{Fe}$ values and Fe content (wt.%) for varying minerals from the Jinchuan ore deposit. Mineral abbreviations: Ol = olivine; Srp = serpentine; Cpx = clinopyroxene; Opx = orthopyroxene; Mag = magnetite; Po = pyrrhotite; Cp = chalcopyrite; Pn = pentlandite.

5. Discussion

To discuss the iron isotope fractionation during the magmatism that leads to the Jinchuan magmatic sulfide Ni-Cu mineralization, it is necessary to understand the processes that developed the net-textured ores. While the origin of such texture remains poorly understood in the literature [18,20], we here offered our understanding in terms of straightforward magmatic processes and physics (Figure 6). The net-textured ores are characterized by euhedral silicate minerals (olivine and pyroxenes prior to serpentinization) surrounded by aggregates of sulfide mineral assemblage (e.g., pyrrhotite, pentlandite, and chalcopyrite) as “interstitial” fills (Figures 3 and 4). Such texture actually represents a snapshot of sulfide-rich mafic magma evolution. This can be readily understood as illustrated in Figure 6.

- (1) A sulfur-rich and sulfide saturated mafic magma led to sulfide melt exsolution/segregation, forming a system of coexisting two-phase liquids, the silicate liquid and the sulfide liquid.
- (2) Since the sulfide liquid has greater density ($>4.00 \text{ g cm}^{-3}$) [51] than the silicate liquid ($\sim 2.75\text{--}2.90 \text{ g cm}^{-3}$) [52], the sulfide liquid will necessarily sink at the base of the “magma chamber” system where the dense sulfide liquid concentrates at the base overlain by the silicate liquid.
- (3) With the higher liquidus temperature, mafic silicate minerals (olivine, orthopyroxene, and clinopyroxene) with densities of $3.25\text{--}3.35 \text{ g cm}^{-3}$ [52] begin to crystallize first and tend to sink at the base of the silicate liquid, but would suspend in the denser sulfide liquid, constituting the network texture.
- (4) Subsequent crystallization of sulfide liquid and solidification of the system results in the observed net-textured Ni-Cu ores above the massive ores and below the disseminated ores in this density/buoyancy controlled scenario.

The above simple and rigorous analyses represent a state-of-the-art understanding of the ore texture development. This is also consistent with the petrography that the silicate mineral assemblages are of cumulate origin as the result of fractional crystallization from the cooling silicate liquid (Figure 6). On the other hand, solidification of the sulfide liquid takes place in situ through equilibrium crystallization (Figure 6). The above reasonable interpretations provide us with a framework to study the difference (if any) of iron isotope compositions between silicate liquid represented by bulk-silicate mineral phases and sulfide liquid represented by bulk-sulfide mineral phases. We also note that during crystallization/solidification of sulfides, iron isotope fractionation must also take place between phases (e.g., [53]). The fact that the iron isotope compositions are essentially the same or rather similar for the same minerals (though from different samples), but distinctly different between minerals as a function of iron content (Figure 5c) suggests that for such a magmatic system, the same mineral phase has a “unique” iron isotope composition. This means that the between-phase iron isotope variation was dominated by equilibrium fractionation with the effect of kinetic fractionation being secondary if not negligible.

5.1. Iron Isotope Composition of Different Iron-Bearing Minerals

Iron sulfides (e.g., pyrrhotite, pentlandite, and chalcopyrite), iron oxides (e.g., chromite and magnetite), and iron-bearing silicate minerals (e.g., olivine, orthopyroxene, and clinopyroxene) are the main iron-bearing minerals in the Jinchuan magmatic Ni-Cu ore deposit. The iron isotope compositions of these minerals varied significantly (Figure 5). The iron isotope compositions of the same minerals show a large range beyond analytical uncertainty. Of all these minerals, pyrrhotite shows strikingly the largest iron isotope composition variation range with all $\delta^{56}\text{Fe}$ values < 0 . Although there were overlaps, between-mineral iron isotope compositional differences were obvious.

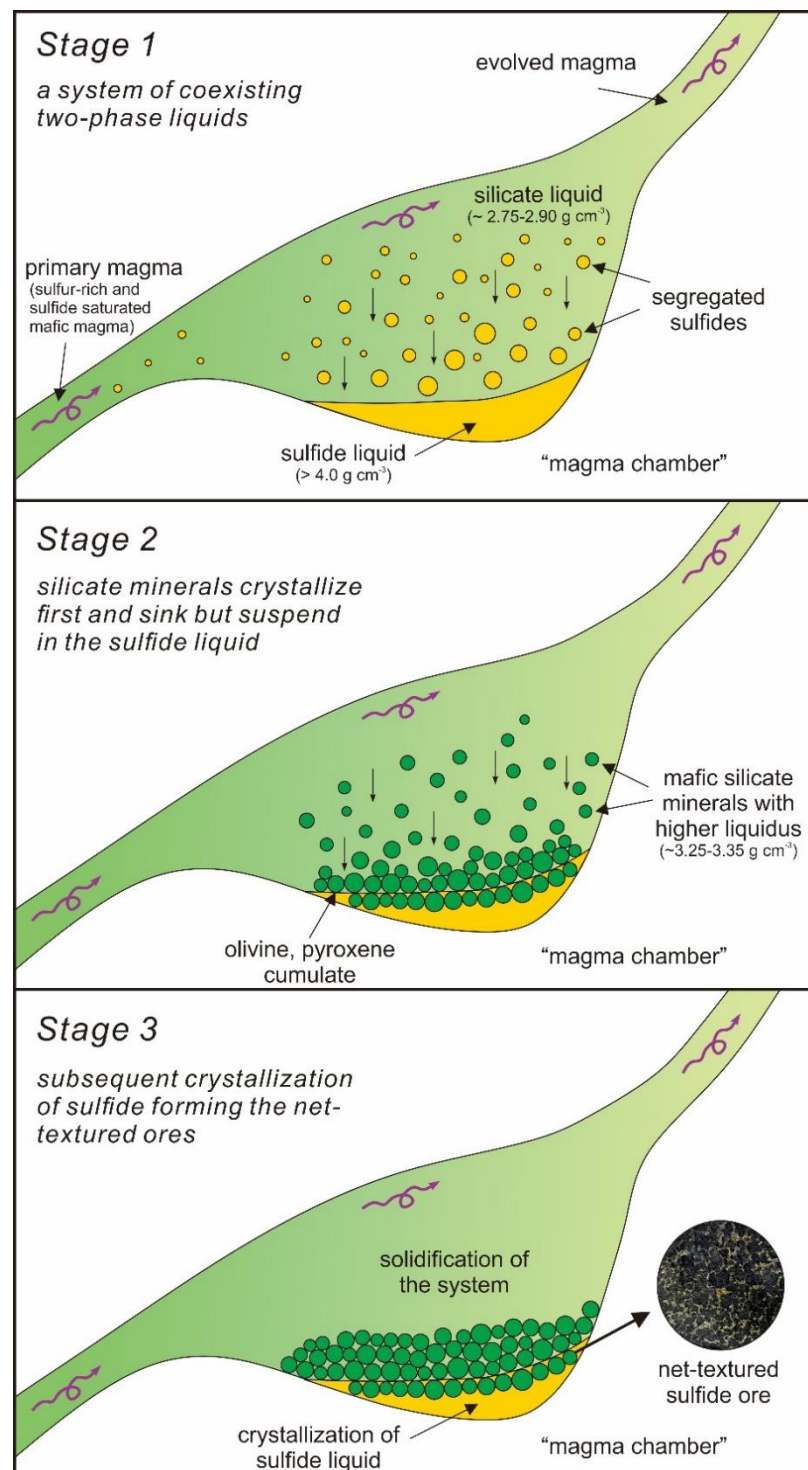


Figure 6. Schematic diagram illustrating the most likely magmatic processes that develop the net-textured ores. Stage 1: a sulfur-rich and sulfide saturated mafic magma led to sulfide melt exsolution/segregation in a “magma chamber”, in which dense (>4.00 g cm⁻³) [51] sulfide liquid droplets sink at the base overlain by the less dense (~2.75–2.90 g cm⁻³) silicate liquid [52]. Stage 2: mafic silicate minerals (olivine, orthopyroxene, and clinopyroxene) have high liquidus temperature than sulfides and higher density (~3.25–3.35 g cm⁻³) than silicate liquid, thus begin to crystallize first and tend to sink at the base of the silicate liquid, but would suspend in the denser sulfide liquid [52]. Stage 3: Subsequent crystallization of sulfide liquid and solidification of the system results in the observed net-textured Ni-Cu ores. It is thus logical to assume that the net-textured sulfide minerals are in equilibrium with the coexisting silicate minerals dominated by olivine.

Given the above analysis on the magma differentiation processes in the “magma chamber” that leads to the network ore texture development as illustrated in Figure 6, it is reasonable to assume that during sulfide-liquid and silicate-liquid segregation prior to their respective crystallization, both liquids must be in equilibrium in terms of iron isotopes although the fractionation factor is unknown (i.e., $\Delta^{56}\text{Fe}_{\text{silicate liquid-sulfide liquid}} = ?$). It is also reasonable to state that the weighted mean iron isotope composition of bulk-sulfide minerals altogether represents that of the sulfide liquid because the solidification of sulfide liquid can be best understood as equilibrium crystallization (see above). On the other hand, as the silicate minerals (dominated by olivine with minor pyroxene) are of cumulate origin resulting from fractional crystallization (see above), the mean iron isotope composition of the bulk-silicate minerals would not represent that of the parental silicate liquid, but can be readily obtained because of the better-constrained fractionation factor (e.g., $\Delta^{56}\text{Fe}_{\text{silicate crystals-melt}} \approx -0.15 \pm 0.05\text{‰}$ [46]). That is, the silicate melt in equilibrium with the sulfide liquid would have $\delta^{56}\text{Fe}$ about $\sim 0.15\text{‰}$ higher than the weighted mean composition of the bulk-silicate minerals. We note that such $\sim 0.15\text{‰}$ difference was negligible compared to the large range of sulfide iron isotope compositional variation for a given mineral and between minerals (Figure 5).

Therefore, the task of unveiling the possible iron isotope fractionation between the silicate liquid and the sulfide liquid in equilibrium was to obtain the weighted mean $\delta^{56}\text{Fe}$ of the bulk-silicate minerals and the weighted mean $\delta^{56}\text{Fe}$ of the bulk-sulfide minerals (see below).

5.1.1. Iron Isotope Compositional Differences between Minerals with Different Valence States

The iron isotope variations among coexisting minerals, if existing, provide convincing evidence for iron isotope fractionation. In the Jinchuan net-textured ores, all the sulfide minerals and silicate minerals (dominated by olivine, orthopyroxene, and minor clinopyroxene) essentially have only Fe^{2+} . Only minor chromite and magnetite may have Fe^{3+} . Serpentinization can produce secondary magnetite, but the fact that all the serpentines took the pseudomorphs of euhedral silicate minerals (Figure 4) with high FeO_T (Table 3) and the fact that only minute secondary magnetite occurred as fine trails in serpentines (Figure 4) indicate that the serpentines retain Fe^{2+} of the original silicate minerals. Hence the bulk-rock ore samples contain only Fe^{2+} with little Fe^{3+} . It has been shown that under equilibrium conditions, heavy Fe isotopes are preferentially associated with high valent Fe^{3+} with shorter bond length and stronger bond strength (i.e., $\text{Fe}^{3+}\text{-O}^{2-}$) over Fe^{2+} with longer bond length and weaker bond strength (i.e., $\text{Fe}^{2+}\text{-O}^{2-}$) and can have up to $\sim 3\text{‰}$ $\delta^{56}\text{Fe}$ fractionation [54–57]. This readily explains the variable heavy Fe with $\delta^{56}\text{Fe} = 0.24\text{--}0.71\text{‰}$ in magnetite, which is important although all the magnetite analyzed is secondary associated with the serpentinization and is volumetrically minute. However, bond strength also depends on ligand types (coordination environments; e.g., $\text{Fe}^{2+}\text{-S}^{2-}$ bond vs. $\text{Fe}^{2+}\text{-O}^{2-}$) [58,59]. Therefore, the iron valent state is not the sole control on iron isotope fractionation between phases under equilibrium conditions. We reiterated that magnetite was secondary and was volumetrically insignificant in these ore samples of the magmatic system that we studied here.

5.1.2. Iron Isotope Compositional Differences between Coexisting Sulfide Minerals

There are few iron isotope data on magmatic sulfides [53]. Like the Sudbury magmatic sulfide deposits, the Jinchuan net-textured ores have three major coexisting sulfide minerals: pyrrhotite (Po), pentlandite (Pn), and chalcopyrite (Cp). The $\delta^{56}\text{Fe}$ values of pure chalcopyrite ($0.09\text{--}0.56\text{‰}$) and pentlandite ($0.53\text{--}1.05\text{‰}$) were both positive, and pentlandite was more enriched in heavy Fe isotopes than chalcopyrite (i.e., $\delta^{56}\text{Fe}(\text{Pn}) > \delta^{56}\text{Fe}(\text{Cp})$). A recent study on magmatic sulfides [53] shows $\delta^{56}\text{Fe}(\text{Po}) < \delta^{56}\text{Fe}(\text{Cp})$ (no data on Pn), with $\delta^{56}\text{Fe}(\text{Po}) < 0$, and $\delta^{56}\text{Fe}(\text{Po})$ ranges from -0.55 to 0.05‰ with the extremely low $\delta^{56}\text{Fe}(\text{Po})$ values of -0.80‰ only found in “impact-related Sudbury deposit”. Our data from the

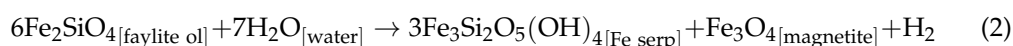
Jinchuan deposit also indicate the low $\delta^{56}\text{Fe}(\text{Po})$, ranging from -1.37 to -0.74% (Tables 5 and 6; Figure 5). Given the same Fe^{2+} in these sulfide minerals, their iron isotope fractionation is most likely controlled by bond length and bond energy. The work by [58] proposed that if the bond lengths of the two minerals are different, their vibration frequencies are correspondingly different. Hence, if there is mass-dependent isotope fractionation between the two minerals, light isotopes will preferentially enter the minerals with longer bond and weaker bond strength. Since pentlandite has the shortest $\text{Fe}^{2+}\text{-S}^{2-}$ bond length and strongest bond strength compared with chalcopyrite and pyrrhotite, while pyrrhotite has the longest bond length [60–64], it is thus consistent that pentlandite is enriched with heavy Fe isotopes than chalcopyrite and pyrrhotite, and pyrrhotite has the lightest Fe isotope composition with $\delta^{56}\text{Fe}(\text{Po}) < 0$.

5.1.3. Iron Isotope Compositions of Primary Silicate Minerals

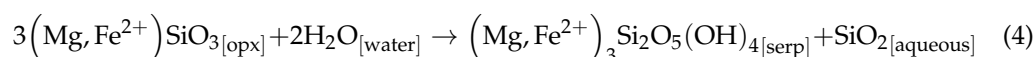
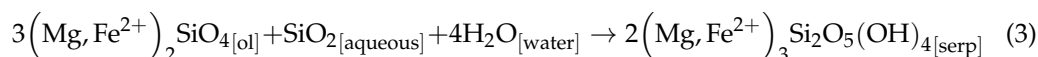
The primary silicate minerals (i.e., olivine (Ol), clinopyroxene (Cpx), and orthopyroxene (Opx)) all have similar $\delta^{56}\text{Fe} = 0.00\text{--}0.01\%$ with small variation ($\delta^{56}\text{Fe}(\text{Ol}) = 0.07 \pm 0.02\%$; $\delta^{56}\text{Fe}(\text{Opx}) = 0.05 \pm 0.03\%$; $\delta^{56}\text{Fe}(\text{Cpx}) = 0.04 \pm 0.01\%$). This small but systematic difference with $\delta^{56}\text{Fe}(\text{Ol}) > \delta^{56}\text{Fe}(\text{Opx}) > \delta^{56}\text{Fe}(\text{Cpx})$ is consistent with being in equilibrium with their parental melt (fertile upper mantle $\delta^{56}\text{Fe} = 0.02 \pm 0.03\%$ [1]) during fractional crystallization at temperatures way above sulfide liquid crystallization (see Figure 6).

5.1.4. Iron Isotope Compositions of Serpentes

Serpentes (Serp) are post-magmatic low-temperature product of serpentinization whose intensity decreases in the order of Ol, Opx, and Cpx [65]. Available studies suggest that serpentes have lighter Fe isotope compositions than the coexisting minerals (Ol, Opx, and Cpx) [66], but our data demonstrate the opposite, i.e., higher $\delta^{56}\text{Fe}(\text{Serp})$ (0.52 ± 0.01 to $0.60 \pm 0.02\%$) $> \delta^{56}\text{Fe}(\text{Ol, Opx, Cpx})$ (0.04 ± 0.01 to $0.07 \pm 0.02\%$). This is an important observation (Table 5; Figure 5). This is expected because serpentinization is often a major disproportionate redox reaction that oxidizes Fe^{2+} (in Serp) into Fe^{3+} (in magnetite) while producing reduced H_2 (e.g., [67]) as follows in terms of iron end-member reaction for conceptual clarity.



Hence, the higher $\delta^{56}\text{Fe}(\text{Serp}) > \delta^{56}\text{Fe}(\text{Ol, Opx, and Cpx})$ could be caused by secondary magnetite dispersed in (and incompletely segregated from) serpentes. However, this interpretation, albeit logical, might be incorrect here because our serpentes had abundant FeO_T (7.7–14.7 wt.%), had network texture intact without deformation, and had little secondary magnetite (Figures 3 and 4), indicating convincingly that the serpentinization in the net-textured samples essentially took place by simple hydration without producing magnetite through the following Ol and Opx hydration reactions:



This simple analysis on the basis of detailed petrography demonstrated that the higher $\delta^{56}\text{Fe}$ in the serpentine ($\delta^{56}\text{Fe}(\text{Serp}) > \delta^{56}\text{Fe}(\text{Ol, Opx, Cpx})$) is real and needs understanding. The above reactions suggest that iron in the serpentine remains as Fe^{2+} , but it is possible that some Fe^{3+} could be “hidden” in the serpentine structures, which needs further investigations. It is also possible that the serpentinization may have produced enhanced $\text{Fe}^{2+}\text{-O}^{2-}$ bond strength. Either or both of the scenarios can help explain why $\delta^{56}\text{Fe}(\text{Serp}) > \delta^{56}\text{Fe}(\text{Ol, Opx, and Cpx})$. These hypothetical scenarios must be examined in future studies.

We found that the serpentinization process that transformed the silicate minerals in questions (Ol > Opx > Cpx) into serpentes is associated with the losses of light Fe

isotopes (e.g., ^{54}Fe), i.e., $\delta^{56}\text{Fe}(\text{Ol, Opx, Cpx}) < \delta^{56}\text{Fe}(\text{Serp})$ (or gains of heavy Fe isotopes (e.g., ^{56}Fe)). Where did the light ^{54}Fe isotope goes to (or heavy $^{56,57}\text{Fe}$ isotopes come from) without volumetrically significant secondary mineral formation associated with the serpentinization (including magnetite)? Considering the contextual relationships among coexisting minerals and mineral chemical/isotopic compositions, we hypothesized that the complementary light Fe isotope must have migrated by diffusion into the coexisting pyrrhotite during serpentinization or at even lower temperatures. It is obvious from petrographical observations (Figure 3) that pyrrhotite is the dominant sulfide mineral packed around the silicate minerals (Serp, Ol, Opx, and Cpx) (Figure 4a,b). This hypothesis can be tested through in situ iron isotope analysis in the future. In this test, we also need to verify our observation of $\delta^{56}\text{Fe}(\text{Pn}) > \delta^{56}\text{Fe}(\text{Cp}) > \delta^{56}\text{Fe}(\text{Po})$ although this order is indeed consistent with the $\text{Fe}^{2+}\text{-S}^{1-2-}$ bond strength decrease due to bond length increase for tetrahedral coordination (Po 2.50 Å, Cp 2.26 Å, and Pn 2.16 Å) [62–64].

5.2. Constructing Iron Isotope Compositions of Coexisting Sulfide Liquid and Silicate Liquid

According to our hypothesized scenario of magma differentiation processes illustrated in Figure 6 and discussion above, we could approximate iron isotope compositions of silicate liquid and sulfide liquid prior to crystallization using weighted mean iron isotope composition of the bulk-silicate minerals and bulk-sulfide minerals respectively. Hence, understanding the iron isotope fractionation between the silicate liquid and sulfide liquid requires iron isotope composition reconstruction of these two liquid phases for the net-textured ore samples (JC-1, 2, and 3). The reconstruction for the bulk-silicate was less demanding because of the similar $\delta^{56}\text{Fe}(\text{Ol, Opx, and Cpx})$ with small variation relative to sulfide minerals. This will form the basis to discuss the possible iron isotope fractionation during the Earth's core formation. Before the iron isotope composition constructions of the two liquids below, a "CIPW" approach (calculate the corresponding mineral composition of ore using chemical compositions of bulk-rock ore and containing minerals; detailed in Table 7; see Appendix C) was used to calculate the content of each mineral (wt.%; sulfide, silicate, oxide, etc.) in net-textured bulk-ores, with the calculated results shown in Table 8.

Table 7. The details of the "CIPW" calculations for the three net-textured ore samples (JC-1, 2, and 3).

Sample no.	Ore-bearing Rock Type	Main Minerals Calculated in Order	Unique Element (mol.%)	The Remaining Elements and Their Contents (mol.%)
JC-1	Sulfide-rich dunite	Chalcopyrite Pentlandite Chromite Serpentine Olivine Pyrrhotite	Chalcopyrite = Cu Pentlandite = Pn chromite = Cr serpentine, olivine = Si, serpentine, olivine = Mg pyrrhotite = Fe	Fe = Fe – Cu, Cu = 0; Fe = Fe – Ni, Ni = 0; Fe = Fe – Cr, Mg = Mg – Cr, Cr = 0; Fe = Fe – Si (serpentine) – Si (olivine), Si = 0, Mg = 0; Fe = 0.
JC-2	sulfide-rich dunite	Chalcopyrite Pentlandite Serpentine Chromite Olivine Pyrrhotite	Chalcopyrite = Cu Pentlandite = Pn serpentine = Al chromite = Cr olivine = Si pyrrhotite = Fe	Fe = Fe – Cu, Cu = 0; Fe = Fe – Ni, Ni = 0; Si = Si – Al, Fe = Fe – Al, Cr = Cr – Al, Al = 0; Fe = Fe – Cr, Cr = 0; Fe = Fe – Si, Si = 0; Fe = 0.
Only serpentine has a lot of Al in JC-2 (unlike chromite of JC-1, which also has a lot of Al)				
JC-3	sulfide-rich lherzolite	Chalcopyrite Pentlandite Chromite Plagioclase Clinopyroxene Orthopyroxene Serpentine Olivine Pyrrhotite	Chalcopyrite = Cu Pentlandite = Pn chromite = Cr plagioclase = Na clinopyroxene = Ca orthopyroxene = Al serpentine, olivine = Si, serpentine, olivine = Mg pyrrhotite = Fe	Fe = Fe – Cu, Cu = 0; Fe = Fe – Ni, Ni = 0; Fe = Fe – Cr, Mg = Mg – Cr, Cr = 0; Ca = Ca – Na, Si = Si – Na, Al = Al – Na, Fe = Fe – Na, Na = 0; Fe = Fe – Ca, Mg = Mg – Ca, Si = Si – Ca, Al = Al – Ca, Ca = 0; Fe = Fe – Al, Mg = Mg – Al, Si = Si – Al, Al = 0; Fe = Fe – Si (serpentine) – Si (olivine), Si = 0, Mg = 0; Fe = 0.

Table 8. Calculated content of each mineral in net-textured ore samples and experimental molecular formula of each mineral.

Sample No.	Mineral Type	Mineral Modal Abundance (wt.%, cal.)	Experimental Molecular Formula
JC-1	Pyrrhotite	13.43	Fe _{0.855} S
	Chalcopyrite	6.734	Cu _{0.944} Fe _{0.959} S ₂
	Pentlandite	6.816	(Fe _{4.531} ,Ni _{3.825}) _{8.355} S ₈
	Serpentine	57.48	(Mg _{5.145} ,Fe _{0.744} ,Mn _{0.060} ,Ti _{0.032} ,Cr _{0.117}) _{6.099} [(Si _{3.570} ,Al _{0.447}) _{4.017} O ₁₀](OH) ₈
	Olivine	13.88	(Mg _{1.720} ,Fe _{0.330}) _{2.049} Si _{0.975} O ₄
	Chromite	1.662	(Mg _{0.165} ,Fe ²⁺ _{0.848} ,Mn _{0.012}) _{1.024} (Cr _{0.890} ,Al _{0.398} ,Fe ³⁺ _{0.664} ,Ti _{0.024}) _{1.976} O ₄
JC-2	Pyrrhotite	14.24	Fe _{0.852} S
	Chalcopyrite	2.945	Cu _{0.912} Fe _{0.930} S ₂
	Pentlandite	10.42	(Fe _{4.125} ,Ni _{4.038}) _{8.164} S ₈
	Serpentine	40.92	(Mg _{5.353} ,Fe _{0.628} ,Cr _{0.033}) _{6.014} [(Si _{3.760} ,Al _{0.300}) _{4.060} O ₁₀](OH) ₈
	Olivine	29.07	(Mg _{1.654} ,Fe _{0.355}) _{2.008} Si _{0.996} O ₄
	Chromite	2.401	(Mg _{0.037} ,Fe ²⁺ _{1.007}) _{1.044} (Cr _{0.409} ,Al _{0.01} ,Fe ³⁺ _{1.503} ,Ti _{0.044}) _{1.956} O ₄
JC-3	Pyrrhotite	4.645	Fe _{0.889} S
	Chalcopyrite	3.286	Cu _{0.885} Fe _{0.948} S ₂
	Pentlandite	2.788	(Fe _{4.026} ,Ni _{3.507}) _{7.533} S ₈
	Serpentine	8.062	(Mg _{4.970} ,Fe ²⁺ _{0.982} ,Mn _{0.021} ,Ca _{0.040}) _{6.014} [(Si _{3.894} ,Fe ³⁺ _{0.132}) _{4.026} O ₁₀](OH) ₈
	Olivine	41.14	(Mg _{1.665} ,Fe _{0.358}) _{2.024} Si _{0.988} O ₄
	Clinopyroxene	8.996	(Na _{0.021} ,Ca _{0.765} ,Mg _{1.040} ,Fe _{0.180} ,Cr _{0.032}) _{2.039} [(Si _{1.859} ,Al _{0.158}) _{2.017} O ₆]
	Orthopyroxene	24.65	(Ca _{0.085} ,Mg _{1.643} ,Fe _{0.283} ,Cr _{0.018}) _{2.028} [(Si _{1.913} ,Al _{0.092}) _{2.004} O ₆]
	Chromite	1.362	(Mg _{0.247} ,Fe ²⁺ _{0.782}) _{1.029} (Cr _{1.000} ,Al _{0.622} ,Fe ³⁺ _{0.320} ,Ti _{0.029}) _{1.971} O ₄
Plagioclase	5.073	(Na _{0.423} ,K _{0.016} ,Ca _{0.559} ,Fe _{0.016}) _{1.014} Al _{1.568} Si _{2.427} O ₈	
JC-4	Pyrrhotite	-	Fe _{0.826} S
	Chalcopyrite	-	Cu _{0.897} Fe _{0.937} S ₂
	Pentlandite	-	(Fe _{3.997} ,Ni _{3.930}) _{7.928} S ₈
	Serpentine	-	(Mg _{4.688} ,Fe _{1.236} ,Ca _{0.018} ,Ni _{0.014}) _{5.956} [(Si _{4.022} O ₁₀)(OH) ₈

The “-” indicates that mineral content is not calculated.

5.2.1. Iron Isotope Compositions of the Silicate Liquid

We assumed that the iron isotope compositions of fresh olivine and pyroxene in JC-3 given in Table 5 can be used to estimate iron isotope compositions of the silicate liquid because of the pervasive serpentinization of sample JC-1 and 2 with almost no fresh silicate separates (Ol, Cpx, and Opx) sufficient for their iron isotope compositions. The $\delta^{56}\text{Fe}$ values of olivine ($0.07 \pm 0.03\%$), orthopyroxene ($0.05 \pm 0.07\%$), and clinopyroxene ($0.04 \pm 0.02\%$) (Table 5) were very close to the chondritic values (Figure 4b).

Since the primary silicate minerals (Ol, Opx, and minor Cpx) are of cumulate origin as the result from fractional crystallization, the iron isotope composition of their parental (equilibrium) melt can be readily obtained using the well understood fractionation factor of $\Delta^{56}\text{Fe}_{\text{silicate (e.g., Ol)-melt}} \approx -0.15 \pm 0.05\%$ [46]. By considering a reasonable mineral mode of 70% Ol, 25% Opx, and 5% Cpx, we can obtain the melt in equilibrium with the cumulate to have $\delta^{56}\text{Fe} = 0.06 + 0.15 \approx 0.21\%$, which is likely to be the maximum by comparing with highest have $\delta^{56}\text{Fe}$ values of global OIB [68]. Note that we do not use serpentines in this construction for reasons elaborated above.

5.2.2. Iron Isotope Compositions of the Sulfide Liquid

As discussed above (see Figure 6), we considered that the sulfide minerals resulted from equilibrium during crystallization. Hence, the weighted mean $\delta^{56}\text{Fe}$ values of the sulfide mineralogy gave a reasonable iron isotope composition of the sulfide liquid. The calculation would be straightforward with caveats on serpentinization associated heavy Fe isotopes depletion (or light Fe isotopes addition) in Po, which was the most abundant sulfide mineral of the net-textured ores.

Similarly, we could calculate the iron isotope composition of the bulk-sulfide phase and thus sulfide liquid (results shown in Table 9; see Appendix B) in the net-textured ore samples according to Equation (1) (Section 4.3 [49,50]) with a “CIPW” approach (detailed in Table 7; results shown in Table 8; see Appendix C). Since the net-textured ore sample JC-3 has only pyrrhotite separate, this will not be discussed.

Table 9. Calculated iron isotope composition of bulk-sulfide phase in net-textured ore samples.

Sample No.	Mineral Type	$\delta^{56}\text{Fe}_i$	$B_1 = \text{Fe Content of Each Mineral}$	$B_2 = \text{Sulfide Content of Bulk-Sulfide Phase}$	$B_3 = \text{Fe Content of Bulk-Sulfide Phase}$	Value of C_i	$\delta^{56}\text{Fe}$ (Sulfide Liquid)			
		% _o , from Part 2 of Table 6	wt.%, from Table 2	wt.%, cal. from Table 8	wt. %	wt.%, Corrected to 100%	Scenario (1), ‰	Scenario (2), ‰	Scenario (3), ‰	Scenario (4), ‰
JC-1	Pyrrhotite	−1.37	59.37	49.77		64.66				
	Chalcopyrite	0.09	30.23	24.96	45.70	16.52	−0.77	−0.39	−0.59	0.32
	Pentlandite	0.53	34.04	25.27		18.82				
	Serpentine	0.60	6.998							
JC-2	Pyrrhotite	−0.74	60.01	51.59		67.75				
	Chalcopyrite	0.56	29.65	10.67	45.70	6.924	−0.20	−0.22	−0.11	0.95
	Pentlandite	1.05	30.67	37.74		25.33				
	Serpentine	0.52	6.015							

$$\delta^{56}\text{Fe} (\text{bulk-sulfide phase}) = \sum C_i \times \delta^{56}\text{Fe}_i \quad (i = \text{each sulfide}); C_i = B_1 \times B_2 / B_3.$$

It should be noted that because of the significantly heavier Fe isotope composition in serpentine and lighter Fe isotope composition in pyrrhotite (Figure 5b), several probable bulk-sulfide (i.e., the sulfide liquid) iron isotope compositions could be estimated (Table 9):

- (1) By excluding the gains of light Fe isotopes for pyrrhotite caused by serpentinization. The $\delta^{56}\text{Fe}$ values of the bulk-sulfide of JC-1 and JC-2 would be -0.77‰ and -0.20‰ , respectively.
- (2) By using pyrrhotite that is less affected by serpentinization in sample JC-3 instead the pyrrhotite in JC-1 and 2, which are strongly serpentinized, the $\delta^{56}\text{Fe}$ values of the bulk-sulfide of JC-1 and JC-2 would be -0.39‰ and -0.22‰ , respectively.
- (3) By taking full consideration of the probable gains of light Fe isotopes for pyrrhotite caused by serpentinization, we could use the difference of iron isotope compositions between the serpentine and average of unaltered silicate minerals ($\delta^{56}\text{Fe} = 0.05\text{‰}$, Ol, Cpx, and Opx) in the net-textured ores, the iron contents of serpentine and pyrrhotite, and the contents of these two minerals in the whole ore respectively to calculate how much lighter are Fe isotope compositions of the pyrrhotite caused by serpentinization as $\Delta^{56}\text{Fe}_{\text{Po}} \times W_{\text{Po}} \times \text{Fe}_{\text{Po}} = \Delta^{56}\text{Fe}_{\text{Serp-Ol}} \times W_{\text{Serp}} \times \text{Fe}_{\text{Serp}}$ ($W_{\text{Po}} = \text{Po content in ore}$; $\text{Fe}_{\text{Po}} = \text{iron content in Po}$; $W_{\text{serp}} = \text{Serp content in ore}$; $\text{Fe}_{\text{serp}}\% = \text{iron content in Serp}$), then take the analytical value plus the $\Delta^{56}\text{Fe}_{\text{Po}}$ calculated above to give the probable value of pyrrhotite before serpentinization as $\delta^{56}\text{Fe}_{\text{Po-before serpentinized}} = \delta^{56}\text{Fe}_{\text{Po-analytical value}} + \Delta^{56}\text{Fe}_{\text{Po}}$. The $\delta^{56}\text{Fe}$ values of the bulk-sulfide of JC-1 and JC-2 would be -0.59‰ and -0.11‰ , respectively.
- (4) If we use pentlandite and chalcopyrite only without including pyrrhotite modified by later serpentinization, we would obtain $\delta^{56}\text{Fe}$ values of the bulk-sulfide of JC-1 and JC-2 to be 0.32‰ and 0.95‰ , respectively.

We did not consider using serpentine to obtain the iron isotope composition of silicate liquid because its heavier Fe isotope composition as the result of probable lighter Fe isotopes losses to pyrrhotite due to serpentinization cannot be ignored although this effect cannot yet be quantified. Hence, we could exclude scenario (1). Since pyrrhotite was the dominant sulfide mineral in net-textured ores, the influence of its iron isotope composition on the total sulfide liquid cannot be ignored. Hence, we could exclude scenario (4). Both (2) and (3) fully considered the significant influence of serpentinization on iron isotopes in the sulfide phase-silicate phase system. Due to the introduction of analytical errors and errors associated with the modal analysis, calculations, and yet to be quantified effect of serpentinization on pyrrhotite and serpentine iron isotope compositions, scenario (3) was less reliable than scenario (2). Since JC-3 was the ore sample with the lowest degree of serpentinization, its iron isotope composition of pyrrhotite might represent more original pyrrhotite. Therefore, we believe that the value obtained by using the value of pyrrhotite from JC-3 to calculate JC-1 and JC-2 was probably closer to the real value, i.e., scenario (2) with an average $\delta^{56}\text{Fe}$ value of $\sim -0.30\text{‰}$.

5.2.3. Differences of Iron Isotopes Between Sulfide Liquid and Silicate Liquid

The above rigorous calculations yield Fe isotope composition for the silicate liquid with $\delta^{56}\text{Fe} \approx 0.21\text{‰}$ and the sulfide liquid with $\delta^{56}\text{Fe} \approx -0.30\text{‰}$, represented by weighted mean value of bulk-sulfide minerals in the net-textured ores (Figure 6).

Therefore, it can be inferred that during the immiscible separation of sulfide liquid and silicate liquid from in the parental sulfide saturated silicate magma, iron isotope fractionation does occur between the two liquids, resulting in the iron isotope compositional differences between sulfide phase and silicate phase. Sulfides tend to preferentially incorporate lighter Fe isotopes, making the iron isotope compositions in sulfide phase lighter than those in the silicate phase. As we reasonably hypothesized from the onset, the final stage of core separation must have been a process of sulfur removal that will not involve iron isotope fractionation (e.g., $(\text{Fe}^{2+}, \text{Ni}^{2+})\text{S}^{2-} \rightarrow (\text{Fe}^0, \text{Ni}^0)_{\text{alloy}} + \text{S}^0$ for conceptual clarity and simplicity) although S and other light elements such as Si and O must still exist in varying small amounts in the core [69].

Previous studies suggest that iron meteorites ($\delta^{56}\text{Fe} = 0.05 \pm 0.02\text{‰}$) have heavier average iron isotope composition compared with chondrites ($\delta^{56}\text{Fe} = -0.01 \pm 0.01\text{‰}$) [2–6]. It is suspected that the specific nature of the bonding between Fe and S in iron meteorites may enhance the affinity for heavy Fe isotopes relative to other phases [70]. The metal phases in the pallasites have a significant heavier iron isotope composition than the co-existing silicate phases [70]. Experimental studies on the separation of metallic phase and silicate melt under 7.7 GPa with 2000 °C and 1 GPa with 1250–1300 °C conditions show no discernible fractionation of iron isotopes between metallic phase and silicate melt phase [12,13]. Based on the crystal lattice parameters of the metallic phase and silicate phase in a diamond anvil experiment, previous researchers found that the calculated iron isotope fractionation factors between the metallic phase and silicate phase have an obvious pressure effect: heavy Fe isotopes enriched in the metal phase compared with the silicate phase at low pressure. On the contrary, light Fe isotopes enriched in the metal phase compared with the silicate phase under the conditions of temperature and pressure at the core mantle boundary (e.g., $P = 130\text{ GPa}$) [16].

While such studies are useful, we reason that (1) the Earth's core formation is not simply a deep mantle process, but must have been a whole-Earth process because Fe depletion is not confined to the deep mantle, but happens to the entire silicate Earth; (2) the strong Fe-S (siderophile property of Fe) and Fe-O (lithophile property of Fe) chemical bonds make it difficult to produce volumetrically significant metal Fe^0 phase in equilibrium with silicate melt; (3) Fe-S sulfide liquid separation from the bulk-silicate Earth thus must be an essential intermediate step; (4) the high density and low viscosity of the Fe-S liquid can thus, under gravity, transport from all Earth depths to the Earth's deep interiors; and (5) a final stage of sulfur removal is expected to complete the metallic core formation. This analysis suggests that determination of Fe isotope differences or similarities of metallic Fe and silicate at whatever pressure conditions without a melt phase (or equilibrium sulfide-silicate liquids) may not provide credible information on Fe isotope fractionation between the Earth's core and the silicate Earth. Therefore, our approach by analyzing Sudbury-type ore minerals is a first step forward for future studies (Figures 1 and 6) despite the fact that the metallic core separation must be a whole-Earth process taking place under all depths. We predict that like net-textured ore sulfides, the Earth's core probably preferentially hosts light iron isotope during the process of core–mantle differentiation (see above our calculated mean values: $\delta^{56}\text{Fe}_{[\text{silicate liquid}]} \approx 0.21\text{‰}$ vs. $\delta^{56}\text{Fe}_{[\text{sulfide liquid}]} \approx -0.30\text{‰}$). If so, the mantle would have a heavier iron isotope composition and the bulk Earth may have $\delta^{56}\text{Fe} < -0.01 \pm 0.01\text{‰}$.

Our discussions on the iron isotope fractionation between immiscible sulfide and silicate liquids were based on the constituent mineral phases of the net-textured ores, in which iron in all phases occurs as Fe^{2+} with no or little Fe^{3+} if any. The magmatic P-T conditions are likely far lower than core–mantle separation conditions. However, the core–mantle separation is unlikely to have taken place at the present-day core and deep

mantle conditions, but throughout the entire Earth, as shallow as the surface of the planet back > 4.5 Ga to as deep as the core depth simply because ~87% Fe of the bulk chondritic Earth would have to sink from all parts and depths of the Earth into the core. Furthermore, this could not take place in the form of metallic Fe to sink through the silicate Earth into the deep Earth, but must have gone through sulfide-silicate liquid segregation as the very first stage. The latter is essential because of the strong $\text{Fe}^{2+}\text{-S}^{2-}$ and $\text{Fe}^{2+}\text{-O}^{2-}$ chemical bonding and because of the strong sulfur affinity of Fe.

Thus, the bulk-silicate phase in our net-textured ore dominated by spinel-facies peridotite can reflect the shallow separation less than 60 km of the early stage, but more probable phases from deeper Earth must be further studied, such as garnet-facies peridotite (60–170 km), whose iron isotope fractionation between coexisting mineral phases may be quite different from the above results. Previous studies suggested that controlled by differences in the coordination environment of cations between coexisting minerals, heavier isotopes are concentrated in lattice positions with stronger bond energy [71,72]. This is maybe why garnet were reported having lighter iron isotope composition than olivine when under an iron isotope balance indicated by analyses on garnet-facies peridotite [54,73–75]. Thus, higher P-T bulk-silicate phases may have lighter iron isotope compositions than those of net-textured ores. Besides, given the preference of heavier iron isotopes to the phases with higher Fe^{3+} or lower Fe^{2+} [9], it is expected that the involvement of Fe^{3+} -bearing minerals (e.g., magnetite and hematite) may lead to heavier iron isotope compositions of these phases.

It is important to note that what we offered in this study is a logical approach by studying actual Earth materials that are accessible and whose formation scenarios (Figures 1 and 6) are physically most plausible towards understanding the process of core–mantle separation and possible Fe isotope fractionation. Our suggested conclusion for a significantly subchondritic Earth in terms of Fe isotopes may need change or refinement. More studies like ours are needed, but we predicted more credible results are expected to come from coexisting sulfide-silicate liquids produced experimentally under varying mantle depth conditions as detailed above.

6. Conclusions

To better understand the iron isotope composition of the bulk Earth, it is unsatisfactory to assume the bulk Earth has the chondritic iron isotope compositions on the basis of oceanic basalts, mantle peridotites, and model mantle compositions because nearly 90 wt.% of the Earth's iron is in the core, which is inaccessible and whose iron isotope composition is unknown. For this reason, we studied iron isotope characteristics of net-textured ores from the Jinchuan magmatic sulfide deposit, which is one of the largest Sudbury-type ore deposits on Earth by analyzing coexisting sulfide (Po, Cp, and Pn) and silicate (Ol, Cpx, and Opx) minerals. The petrography, analytical data, and rigorous discussion above allowed us to reach the following conclusions with suggested future works:

- (1) There were three major sulfide minerals (pyrrhotite (Po), chalcopyrite (Cp), and pentlandite (Pn)) in the net-textured ores. The $\delta^{56}\text{Fe}$ value of these sulfides varied greatly: $-1.37\text{--}-0.74\text{‰}$ (Po) < $0.09\text{--}0.56\text{‰}$ (Cp) < $0.53\text{--}1.05\text{‰}$ (Pn).
- (2) The silicate minerals were all of cumulate origin, dominated by olivine (Ol) with a small amount of pyroxene (clinopyroxene (Cpx) < orthopyroxene (Opx)). Their $\delta^{56}\text{Fe}$ values were $0.07 \pm 0.03\text{‰}$ (Ol) > $0.05 \pm 0.07\text{‰}$ (Opx) > $0.04 \pm 0.02\text{‰}$ (Cpx), which were all close to the chondritic values.
- (3) By assuming that the coexisting sulfide and silicate minerals of net-textured ores were crystallized/solidified from respective sulfide and silicate liquids segregated from the sulfur-rich and sulfide-saturated parental magma, and by reconstructing the weighted mean iron isotope compositions of bulk-sulfide minerals and bulk-silicate minerals, we obtained the iron isotope composition of the silicate liquid ($\delta^{56}\text{Fe} \approx 0.21\text{‰}$) in equilibrium with the silicate minerals (Ol, Cpx, and Opx) and the iron isotope composition of the sulfide liquid ($\delta^{56}\text{Fe} \approx -0.30\text{‰}$), which was the best value

possible with caveats, including the effect of serpentinization that must have resulted in heavy Fe isotope enrichment in serpentines while light Fe isotope enrichment in the coexisting pyrrhotite.

- (4) Our preferred scenario of core formation was through silicate-sulfide liquid segregation followed by sulfur removal. The sulfide liquid iron isotope composition was expected to be the same as the metallic core. Thus, there must be iron isotope fractionation between the metallic core and the silicate mantle according to the significant differences of iron isotope composition between the sulfide liquid and silicate liquid obtained from the Jinchuan net-textured sulfide ore samples with the fractionation factor of $\Delta^{56}\text{Fe}_{\text{silicate-sulfide}} \approx 0.51\text{‰}$. If we simply compared the difference between the weighted mean bulk-silicate minerals of $\delta^{56}\text{Fe}_{(0.70\text{ol},0.25\text{opx},0.05\text{cpx})} = 0.06\text{‰}$ with weighted mean bulk-sulfide minerals of $\delta^{56}\text{Fe} \approx -0.30\text{‰}$, we would have $\Delta^{56}\text{Fe}_{\text{silicate-sulfide}} \approx 0.36\text{‰}$. This is still a rather large difference and we do not intend to claim this value to be correct, but emphasize that iron isotope fractionation does take place between silicates and sulfides in the Sudbury-type magmatic sulfide mineralization. We thus hypothesized that iron isotope fractionation must take place during core–mantle separation, and predicted that the bulk Earth must have significantly lighter Fe isotope composition than the chondrites (i.e., $\delta^{56}\text{Fe} < -0.01 \pm 0.01\text{‰}$). We predicted that the Fe isotope analysis of coexisting sulfide-silicate liquids produced experimentally under varying mantle depth conditions will complement the study of the type we reported here and altogether helped provide credible Fe isotope compositions of the bulk-Earth and the possible Fe isotope differences between the Earth's core and the silicate Earth.

The importance of our study was to advocate that the Sudbury-type net-textured ores are the best materials available for studying potential core–mantle iron isotope fractionation and to bring about an impetus for further study towards better understanding the chemical and isotopic differentiation of the Earth. It is worthy to note that serpentinization in net-textured ores is characterized by hydration of olivine (and Opx), which seems to be a process of losing light Fe isotopes or gaining heavy Fe isotopes through re-equilibration with the coexisting pyrrhotite, as the pyrrhotite gains light Fe isotopes from serpentines or loses heavy Fe isotopes to serpentines. This is a reasonable interpretation, but must be tested through in situ Fe isotope profile studies. Although we did not analyze Ni isotopes, because of the close Fe-Ni association in the magmatic mineralization and because of the majority of Earth's Ni is also in the core, we inferred that Ni isotope fractionation must also have taken place during the core separation. The Ni isotope study will complement our Fe isotope study towards improved understanding of the Earth's core separation.

Author Contributions: Y.N. designed the project, P.W. and Y.N. wrote the manuscript, P.W. did analysis with the assistance of P.S., X.W., P.G., H.G. and M.D. F.S., Y.S., S.X., Y.C. and L.S. contributed to the discussion. All authors have read and agreed to the published version of the manuscript.

Funding: This study is supported by the National Science Foundation of China (NSFC, 41630968, 91958215), the NSFC-Shandong Joint Fund for Marine Science Research Centers (U1606401), and 111 Project (B18048).

Data Availability Statement: The data presented in this study are available in the text.

Conflicts of Interest: The authors declare no conflict of interest.

Appendix A

The content of each sulfide mineral in the impure mineral separates (i.e., mixture of three sulfide minerals) can be calculated by the following steps:

- (1) The weight percentages of the major elements FeO_T , CuO , and NiO in the impure mineral separates (wt.%; Table 4) are converted into the mole percentages of the elements Fe, Cu, and Ni (mol.%);

- (2) According to the empirical molecular formulae given by different sulfides in Table 2, the mole percentage of the element is converted into the mineral molecular percentage (mol.%). Assuming that the coefficients of Fe, Cu, and Ni in the empirical molecular formula of sulfide are x , y , and z respectively, the general molecular formula can be expressed as $Fe_xCu_yNi_zS_n$, which gives pyrrhotite as $Fe_{x1}Cu_{y1}Ni_{z1}S$, chalcopyrite as $Fe_{x2}Cu_{y2}Ni_{z2}S_2$, and pentlandite as $Fe_{x3}Cu_{y3}Ni_{z3}S_8$; Pentlandite (mol.%) = Ni (mol.%) / $z \times 3$, chalcopyrite (mol.%) = Cu (mol.%) / $y \times 2$, Fe content of Pyrrhotite (mol.%) = Total Fe – $x \times 3 \times$ Pentlandite (mol.%) – $x \times 2 \times$ chalcopyrite (mol.%), and Pyrrhotite (mol.%) = Fe content of Pyrrhotite (mol.%) / $x \times 1$.
- (3) The mole percentage of each sulfide and its empirical molecular formula (Table 2) are converted to the mass percentage (wt.%) of each sulfide, and then normalized to 100%. Sulfide (wt.%) = Sulfide (mol.%) \times The relative molecular mass of the empirical molecular formula $\times 100\%$.

Appendix B

According to Equation (1), we could calculate the iron isotope composition of various constituent minerals ($\delta^{56}Fe_i$) from the iron isotope composition of the bulk-rock ($\delta^{56}Fe$) and mass fraction of iron of each mineral (C_i) in the total iron of the bulk-rock through the following calculation steps (by assuming that impure sulfide mineral separates are the “bulk-rock” ($\delta^{56}Fe$) and various pure sulfide end-members are “constituent minerals” ($\delta^{56}Fe_i$):

Let A_1 = Fe content in each mineral (wt.%), A_2 = mineral content in the bulk rock (wt.%), and A_3 = Fe content in the bulk-rock (wt.%), then $C_i = A_1 \times A_2 / A_3$, normalized to 100%. Assuming that the impure mineral separate is the “bulk-rock”, we had $\delta^{56}Fe$ (impure mineral separate) = $C_{Po} \times \delta^{56}Fe(Po) + C_{Cp} \times \delta^{56}Fe(Cp) + C_{Pn} \times \delta^{56}Fe(Pn)$. Part 2 of Table 6 gives A_1 values for each sulfide mineral measured using EMPA (Table 2). Table 6 gives A_2 values for each sulfide mineral in impure mineral separate as calculated above. Table 6 also gives A_3 values in that impure mineral separate (Tables 4 and 6). Thus, we could obtain the iron isotope compositions of pure sulfide end-members ($\delta^{56}Fe_i$; Part 2 of Table 6).

Similarly, we could calculate the iron isotope composition of the bulk-sulfide phase in the net-textured ore samples according to Equation (1) with a “CIPW” approach (see Appendix C for details) as follows: $\delta^{56}Fe$ (bulk-sulfide) = $C_{Po} \times \delta^{56}Fe(Po) + C_{Cp} \times \delta^{56}Fe(Cp) + C_{Pn} \times \delta^{56}Fe(Pn)$. The $\delta^{56}Fe$ of each sulfide uses the pure end-member iron isotopes calculated in Section 4.3 ($\delta^{56}Fe_i$; Part 2 of Table 6). By letting B_1 = Fe content in each sulfide mineral (wt.%; Tables 2 and 9) and B_2 = each sulfide mineral content in the total sulfide (wt.%), we can obtain Fe content of total sulfides (wt.%; $B_3 = \Sigma(B_1 \times B_2) \times 100$) and thus $C_i = B_1 \times B_2 / B_3$ (Table 9). With all these, we can obtain possible bulk-sulfide and thus sulfide liquid iron isotope compositions given in Table 9. Since the net-textured ore sample JC-3 has only pyrrhotite separate, this will not be discussed.

Appendix C

The iron isotope fractionation is most likely to take place at the magmatic molten stage with sulfide liquid exsolved or segregated from the sulfur and sulfide saturated silicate liquid. In this model scenario (Figure 6), there is expected to be little iron isotope fractionation between silicate minerals and sulfide minerals with the exception of serpentine-pyrrhotite (see above and below). The bulk-silicate minerals (prior to serpentinization) represent iron isotope composition of the silicate liquid with the consideration of $\Delta^{56}Fe_{\text{crystal-melt}} \approx -0.15$ [36]. The bulk-sulfide minerals (except for pyrrhotite (Po)) represent the iron composition of the sulfide liquid from which they crystallized. Hence, to understand the iron isotope fractionation between the silicate liquid and sulfide liquid requires reconstruction of bulk-sulfide iron isotope composition for the net-textured ore samples (JC-1, 2, and 3). Determination of the iron isotope composition of the bulk-silicate

is easier because of the similar $\delta^{56}\text{Fe}$ (Ol, Opx, and Cpx) with small variation relative to sulfide minerals.

A “CIPW” approach was used to obtain the sulfide modal abundances of the net-textured ore samples from Jinchuan deposit using chemical formula of minerals calculated from major element analyses (Tables 2–4 and 8). The specific procedures are as follows:

- (1) The major ore elements (such as FeO, CuO, and Cr_2O_3 in wt.%; Table 4) in the bulk-ore samples (JC-1, 2, and 3) are converted to their molar percentages (such as Fe, Cu, and Cr in mol.%).
- (2) The modal mineralogy in mol.% can be calculated using the unique element of each mineral (e.g., Ni in pentlandite, Cu in chalcopyrite, Cr in chromite, etc.). For the elements common in all minerals, simultaneous equations are used.
- (3) Since pyrrhotite only contains Fe and S, its modal calculation is done after the modes of all other iron-bearing minerals are completed using the residual Fe of total Fe minus all the Fe already used so as to obtain the modes of all the major minerals in the net-textured ore samples.

It should be noted that: (1) The equal sign only means that the mineral (mol.%) can be calculated using a single element (mol.%) and the molecular formula of that mineral with the coefficient of each element in the molecular formula omitted in each equation. Take the chalcopyrite of sample JC-1 ($\text{Cu}_{0.944}\text{Fe}_{0.959}\text{S}_2$) as an example, chalcopyrite = Cu, which is actual chalcopyrite = $\text{Cu}/0.944$; (2) the equation follows the computer code tradition, e.g., $\text{Fe} = \text{Fe} + \text{Cu} + \text{Ni}$, means sum Fe, Cu, and Ni to replace the current Fe value; and (3) the coefficients obtained from the mineral molecular formula are omitted for clarity. For example, for the chalcopyrite of JC-1 ($\text{Cu}_{0.944}\text{Fe}_{0.959}\text{S}_2$), $\text{Fe} = \text{Fe} - \text{Cu}$, which is actually $\text{Fe} = \text{Fe} - 0.959/0.944 \times \text{Cu}$. The details of the above calculations for the three samples (JC-1, 2, and 3) are given in Table 7.

- (4) Then, convert the molar percentage of each mineral in the bulk-ore samples into weight percentage (wt.%) using the molecular formulae (Table 8): Each mineral (wt.%) = each mineral (mol.%) \times relative molecular weight in the experimental molecular formula;
- (5) Normalize the above to 100%.

The calculated mineral modal abundances for the three net-textured ore samples (JC-1, 2, and 3) were given in Table 8. The calculated mineral models were similar to petrographic estimates for these samples given in Table 1.

References

1. Weyer, S.; Ionov, D.A. Partial melting and melt percolation in the mantle: The message from Fe isotopes. *Earth Planet. Sci. Lett.* **2007**, *259*, 119–133. [[CrossRef](#)]
2. Schoenberg, R.; von Blanckenburg, F. Modes of planetary-scale Fe isotope fractionation. *Earth Planet. Sci. Lett.* **2006**, *252*, 342–359. [[CrossRef](#)]
3. Zhu, X.K.; Guo, Y.L.; O’Nions, R.K.; Yound, E.D.; Ash, R.D. Isotopic homogeneity of iron in the early solar nebula. *Nature* **2001**, *412*, 311–313. [[CrossRef](#)] [[PubMed](#)]
4. Poitrasson, F.; Freydier, R. Heavy iron isotope composition of granites determined by high resolution MC-ICP-MS. *Chem. Geol.* **2005**, *222*, 132–147. [[CrossRef](#)]
5. Hezel, D.C.; Needham, A.W.; Armytage, R.; Georg, B.; Abel, R.L.; Kurahashi, E.; Coles, B.J.; Rehkamper, M.; Russell, S.S. A nebula setting as the origin for bulk chondrule Fe isotope variations in CV chondrites. *Earth Planet. Sci. Lett.* **2010**, *196*, 423–433. [[CrossRef](#)]
6. Dauphas, N.; Craddock, P.R.; Asimow, P.D.; Bennett, V.C.; Nutman, A.P.; Ohnenstetter, D. Iron isotopes may reveal the redox conditions of mantle melting from Archean to Present. *Earth Planet. Sci. Lett.* **2009**, *288*, 255–267. [[CrossRef](#)]
7. Wang, Y.; Zhu, X.K. Fe isotope systematics and its implications in ore deposit geology. *Acta Petrol. Sin.* **2012**, *28*, 3638–3654. (In Chinese)
8. Poitrasson, F.; Halliday, A.N.; Lee, D.C.; Lvasseur, S.; Teutsch, N. Iron isotope differences between Earth, Moon, Mars and Vesta as possible records of contrasted accretion mechanisms. *Earth Planet. Sci. Lett.* **2004**, *223*, 253–266. [[CrossRef](#)]
9. Dauphas, N.; John, S.G.; Rouxel, O. Iron isotope systematics. *Rev. Mineral. Geochem.* **2017**, *82*, 415–510. [[CrossRef](#)]

10. Dauphas, N.; Roskosz, M.; Alp, E.; Golden, D.; Sio, C.; Tissot, F.; Hu, M.; Zhao, J.; Gao, L.; Morris, R. A general moment NRIXS approach to the determination of equilibrium Fe isotopic fractionation factors: Application to goethite and jarosite. *Geochim. Cosmochim. Acta* **2012**, *94*, 254–275. [[CrossRef](#)]
11. Dauphas, N.; Roskosz, M.; Alp, E.; Neuville, D.; Hu, M.; Sio, C.; Tissot, F.; Zhao, J.; Tissandier, L.; Médard, E. Magma redox and structural controls on iron isotope variations in Earth's mantle and crust. *Earth Planet. Sci. Lett.* **2014**, *398*, 127–140. [[CrossRef](#)]
12. Poitrasson, F.; Roskosz, M.; Corgne, A. No iron isotope fractionation between molten alloys and silicate melt to 2000 °C and 7.7 GPa: Experimental evidence and implications for planetary differentiation and accretion. *Earth Planet. Sci. Lett.* **2009**, *278*, 376–385. [[CrossRef](#)]
13. Hin, R.C.; Schmidt, M.W.; Bourdon, B. Experimental evidence for the absence of iron isotope fractionation between metal and silicate liquids at 1 GPa and 1250–1300 °C and its cosmochemical consequences. *Geochim. Cosmochim. Acta* **2012**, *93*, 164–181. [[CrossRef](#)]
14. Shahar, A.; Hillgren, V.; Horan, M.; Mesa-Garcia, J.; Kaufman, L.; Mock, T. Sulfur-controlled iron isotope fractionation experiments of core formation in planetary bodies. *Geochim. Cosmochim. Acta* **2015**, *150*, 253–264. [[CrossRef](#)]
15. Shahar, A.; Schauble, E.A.; Caracas, R.; Gleason, A.E.; Reagan, M.M.; Xiao, Y.; Shu, J.; Mao, W. Pressure-dependent isotopic composition of iron alloys. *Science* **2016**, *352*, 580–582. [[CrossRef](#)]
16. Polyakov, V.B. Equilibrium iron isotope fractionation at core-mantle boundary conditions. *Science* **2009**, *323*, 912–914. [[CrossRef](#)] [[PubMed](#)]
17. Liu, J.; Dauphas, N.; Roskosz, M.; Hu, M.Y.; Yang, H.; Bi, W.; Zhao, J.; Alp, E.E.; Hu, J.Y.; Lin, J.F. Iron isotopic fractionation between silicate mantle and metallic core at high pressure. *Nat. Commun.* **2017**, *8*, 14377. [[CrossRef](#)] [[PubMed](#)]
18. Naldrett, A.J. *Magmatic sulfide deposits: Geology, Geochemistry and Exploration*; Springer: Berlin/Heidelberg, Germany, 2004.
19. Naldrett, A.J. A portion of the system Fe-S-O between 900 and 1080 °C and its application to sulfide ore magmas. *J. Petrol.* **1969**, *10*, 171–201. [[CrossRef](#)]
20. Naldrett, A.J. Nickel sulfide deposits-their classification and genesis with special emphasis on deposits of volcanic association. *Can. Inst. Min. Metall. Bull.* **1973**, *66*, 45–63.
21. Naldrett, A.J. World-class Ni-Cu-PGE deposits: Key factors in their genesis. *Miner. Depos.* **1999**, *34*, 227–240. [[CrossRef](#)]
22. Jia, E.H. Geological characteristics of the Jinchuan Cu-Ni sulfide deposit in Gansu province. *Miner. Deposits* **1986**, *5*, 27–38. (In Chinese)
23. Yu, W.J.; Gao, Q.; Zhang, Z.P.; Jin, X.Q.; Deng, D.Q. Characteristics experimental of surrounding rock mass in tectonic zone and its rheological law analysis. *J. Cent. South Univ. (Sci. Technol.)* **2009**, *40*, 1086–1091. (In Chinese)
24. Tang, Z.L.; Li, W.Y. *Mineralization model and geology of the Jinchuan PGE-bearing deposit*; Geological Publishing House: Beijing, China, 1995; pp. 1–205. (In Chinese)
25. Song, S.G.; Niu, Y.L.; Su, L.; Xia, X.H. Tectonics of the North Qilian orogen, NW China. *Gondwana Res.* **2013**, *23*, 1378–1401. [[CrossRef](#)]
26. Li, C.; Xu, Z.; Waal, S.A.D.; Ripley, E.M.; Maier, W.D. Compositional variations of olivine from the Jinchuan Ni-Cu sulfide deposit, western China: Implications for ore genesis. *Miner. Depos.* **2004**, *39*, 159–172. [[CrossRef](#)]
27. Zhang, M.J.; Tang, Q.Y.; Hu, P.Q.; Ye, X.R.; Cong, Y.N. Noble gas isotopic constraints on the origin and evolution of the Jinchuan Ni-Cu-(PGE) sulfide ore-bearing ultramafic intrusion, western China. *Chem. Geol.* **2013**, *339*, 301–312. [[CrossRef](#)]
28. Yang, G.; Du, D.A.; Lu, J.R.; Qu, W.J.; Chen, J.F. Re-Os (ICP-MS) dating of massive sulfide ore in Jinchuan Ni-Cu-Pt deposit. *Sci. China Ser. D Earth Sci.* **2005**, *35*, 241–245. (In Chinese)
29. Yan, H.Q.; Su, S.G.; Jiao, J.G.; Tang, H. Metallogenic epoch of Jinchuan Cu-Ni (PGE) magmatic sulfide deposit. *Earth Sci. Front.* **2005**, *12*, 309–315. (In Chinese)
30. Li, X.H.; Su, L.; Chung, S.L.; Li, Z.X.; Liu, Y.; Song, B.; Liu, D.Y. Formation of the Jinchuan ultramafic intrusion and the world's third largest Ni-Cu sulfide deposit: Associated with the ~825 Ma south China mantle plume? *Geochem. Geophys. Geosyst.* **2005**, *6*. [[CrossRef](#)]
31. Tian, Y.L.; Wu, S.J.; Meng, R.; Wang, Y.S.; Lin, C.L.; Xiao, L.Z. La-ICPMS Zircon U-Pb age of the Jinchuan ultramafic intrusion. *Acta Mineral. Sin.* **2007**, *27*, 211–217. (In Chinese)
32. Tang, Z.L.; Yang, J.D.; Xu, S.J.; Tao, X.C.; Li, W.Y. Sm-Nd Dating of Jinchuan Ore-bearing Ultramafic rock. *Chin. Sci. Bull.* **1992**, *37*, 918–920. (In Chinese)
33. Peng, P.; Liu, W.J.; Zhai, M.G. Response of north China block to Rodinia supercontinent and its characteristics. *Acta Petrol. Mineral.* **2002**, *21*, 342–355. (In Chinese)
34. Li, X.H.; Su, L.; Song, B.; Liu, D.Y. Jinchuan ultramafic intrusive SHRIMP zircon U-Pb age and its geological significance. *Chin. Sci. Bull.* **2004**, *49*, 401–402. (In Chinese)
35. Li, W.Y.; Yang, P.F. Late Neoproterozoic sedimentations of the carbonate-detrital flows in Longshou mountains, northwest China: Implications for its tectonic environments. *Acta Sedimentol. Sin.* **2004**, *22*, 142–146. (In Chinese)
36. Zhang, M.J.; Kamo, S.L.; Chusi, L.; Hu, P.Q.; Edward, M.R. Precise U-Pb zircon-baddeleyite age of the Jinchuan sulfide ore-bearing ultramafic intrusion, Western China. *Miner. Depos.* **2010**, *45*, 3–9. [[CrossRef](#)]
37. Ai, Q.X.; Zeng, R.Y.; He, Q.J.; Lai, J.Q.; Mao, X.C. Geochronology and Zircon Hf Isotope of Meta-basic rocks from Jinchuan Mineral Area and Its Geological Significance. *Acta Mineral. Sin.* **2018**, *389*, 185–195.

38. Yan, H.Q.; Liu, Q.F.; Tang, Z.L.; Fan, M.C.; Wang, Q.; Ren, J.M.; Fan, C.F. Structural properties of the Longshoushan block: Constraint from LA-ICP-MS U-Pb zircon dating. *Eng. Sci.* **2015**, *17*, 59–72. (In Chinese) [[CrossRef](#)]
39. Liu, Y.S.; Hu, Z.C.; Gao, S.; Günther, D.; Xu, J.; Gao, C.G.; Chen, H.H. In situ analysis of major and trace elements of anhydrous minerals by LA-ICP-MS without applying an internal standard. *Chem. Geol.* **2008**, *257*, 34–43. [[CrossRef](#)]
40. Chen, L.; Liu, Y.S.; Hu, Z.C.; Gao, S.; Zong, K.Q.; Chen, H.H. Accurate determinations of fifty-four major and trace elements in carbonate by LA-ICP-MS using normalization strategy of bulk components as 100%. *Chem. Geol.* **2011**, *284*, 283–295. [[CrossRef](#)]
41. Kong, J.J.; Niu, Y.L.; Sun, P.; Xiao, Y.Y.; Guo, P.Y.; Hong, D.; Zhang, Y.; Shao, F.L.; Wang, X.H.; Duan, M. The origin and geodynamic significance of the Mesozoic dykes in eastern continental China. *Lithos* **2019**, *332*, 328–339. [[CrossRef](#)]
42. Chen, S.; Wang, X.H.; Niu, Y.L.; Sun, P.; Duan, M.; Xiao, Y.Y.; Guo, P.Y.; Gong, H.M.; Wang, G.D.; Xue, Q.Q. Simple and cost-effective methods for precise analysis of trace element abundances in geological materials with ICP-MS. *Sci. Bull.* **2017**, *62*, 277–289. [[CrossRef](#)]
43. Gong, H.M.; Guo, P.Y.; Chen, S.; Duan, M.; Sun, P.; Wang, X.H.; Niu, Y.L. A re-assessment of nickel-doping method in iron isotope analysis on rock samples using multi-collector inductively coupled plasma mass spectrometry. *Acta Geochim.* **2020**, *39*, 355–364. [[CrossRef](#)]
44. Oeser, M.; Weyer, S.; Horn, I.; Schuth, S. High-precision Fe and Mg isotope ratios of silicate reference glasses determined in situ by femtosecond LA-MC-ICP-MS and by solution nebulization MC-ICP-MS. *Geostand. Geoanal. Res.* **2014**, *38*, 311–328. [[CrossRef](#)]
45. Chen, K.Y.; Yuan, H.L.; Liang, P.; Bao, Z.A.; Chen, L. Improved nickel-corrected isotopic analysis of iron using high-resolution multi-collector inductively coupled plasma mass spectrometry. *Int. J. Mass Spectrom.* **2017**, *421*, 196–203. [[CrossRef](#)]
46. Chen, S.; Niu, Y.L.; Guo, P.Y.; Gong, H.M.; Sun, P.; Xue, Q.Q.; Duan, M.; Wang, X.H. Iron isotope fractionation during mid-ocean ridge basalt (MORB) evolution: Evidence from lavas on the East Pacific Rise at 10°30'N and its implications. *Geochim. Cosmochim. Acta* **2019**, *267*, 227–239. [[CrossRef](#)]
47. He, Y.; Ke, S.; Teng, F.Z.; Wang, T.; Wu, H.; Lu, Y.; Li, S. High-precision iron isotope analysis of geological reference materials by high-resolution MC-ICP-MS. *Geostand. Geoanal. Res.* **2015**, *39*, 341–356. [[CrossRef](#)]
48. Craddock, P.R.; Dauphas, N. Iron isotopic compositions of geological reference materials and chondrites. *Geostand. Geoanal. Res.* **2011**, *35*, 101–123. [[CrossRef](#)]
49. Ye, H.; Wu, C.Z.; Yang, T.; Santosh, M.; Yao, X.Z.; Gao, B.F.; Wang, X.L.; Li, W. Updating the Geologic Barcodes for South China: Discovery of Late Archean Banded Iron Formations in the Yangtze Craton. *Sci. Rep.* **2017**, *7*, 1–9. [[CrossRef](#)]
50. Ye, H.; Wu, C.Z.; Brzozowski, M.J.; Yang, T.; Zha, X.P.; Zhao, S.G.; Gao, B.F.; Li, W.Q. Calibrating equilibrium Fe isotope fractionation factors between magnetite, garnet, amphibole, and biotite. *Geochim. Cosmochim. Acta* **2020**, *271*, 78–95. [[CrossRef](#)]
51. Mungall, J.E.; Su, S. Interfacial tension between magmatic sulfide and silicate liquids: Constraints on kinetics of sulfide liquation and sulfide migration through silicate rocks. *Earth Planet. Sci. Lett.* **2005**, *234*, 135–149. [[CrossRef](#)]
52. Niu, Y.L.; Batiza, R. In-situ densities of silicate melts and minerals as a function of temperature, pressure, and composition. *J. Geol.* **1991**, *99*, 767–775. [[CrossRef](#)]
53. Bilinker, L.D.; Weis, D.; Scoates, J.S.; Perry, E. The application of stable Fe isotopes to magmatic sulfide systems: Constraints on the Fe isotope composition of magmatic pyrrhotite. *Econ. Geol.* **2018**, *113*, 1181–1192. [[CrossRef](#)]
54. Beard, B.L.; Johnson, C.M. Inter-mineral Fe isotope variations in mantle-derived rocks and implications for the Fe geochemical cycle. *Geochim. Cosmochim. Acta* **2004**, *68*, 4727–4743. [[CrossRef](#)]
55. Johnson, C.M.; Skulan, J.L.; Beard, B.L.; Sun, H.; Nealon, K.H.; Braterman, P.S. Isotopic fractionation between Fe (III) and Fe (II) in aqueous solutions. *Earth Planet. Sci. Lett.* **2002**, *195*, 141–153. [[CrossRef](#)]
56. Welch, S.A.; Beard, B.L.; Johnson, C.M.; Braterman, P.S. Kinetic and equilibrium Fe isotope fractionation between aqueous Fe (II) and Fe (III). *Geochim. Cosmochim. Acta* **2003**, *67*, 4231–4250. [[CrossRef](#)]
57. Wiesli, R.A.; Beard, B.L.; Johnson, C.M. Experimental determination of Fe isotope fractionation between aqueous Fe (II), siderite, and green rust in abiotic system. *Chem. Geol.* **2004**, *221*, 343–362. [[CrossRef](#)]
58. Sossi, P.A.; O'Neill, H.S.C. The effect of bonding environment on iron isotope fractionation between minerals at high temperature. *Geochim. Cosmochim. Acta* **2017**, *196*, 121–143. [[CrossRef](#)]
59. Wei, Y.Q.; Niu, Y.L.; Gong, H.M.; Duan, M.; Chen, S.; Guo, P.Y.; Sun, P. Geochemistry and iron isotope systematics of coexisting Fe-bearing minerals in magmatic Fe-Ti deposits: A case study of the Damiao titanomagnetite ore deposits, North China Craton. *Gondwana Res.* **2020**, *81*, 240–251. [[CrossRef](#)]
60. Fujisawa, M.; Suga, S.; Mizokawa, T.; Fujimori, A.; Sato, K. Electronic structures of CuFeS₂ and CuAl_{0.9}Fe_{0.1}S₂ studied by electron and optical spectroscopies. *Phys. Rev. B* **1994**, *49*, 7155. [[CrossRef](#)]
61. Chauke, H.R.; Nguyen-Manh, D.; Ngoepe, P.E.; Pettifor, D.G.; Fries, S.G. Electronic structure and stability of the pentlandites Co₉S₈ and (Fe, Ni)₉S₈. *Phys. Rev. B* **2002**, *66*, 155105. [[CrossRef](#)]
62. Sakkopoulos, S.; Vitoratos, E.; Argyreas, T. Correlation between chemical bonds and properties in pyrrhotite. *J. Chem. Educ.* **1986**, *63*, 665. [[CrossRef](#)]
63. Gibbs, G.V.; Cox, D.F.; Rosso, K.M.; Ross, N.L.; Downs, R.T.; Spackman, M.A. Theoretical electron density distributions for Fe- and Cu-sulfide earth materials: A connection between bond length, bond critical point properties, local energy densities, and bonded interactions. *J. Phys. Chem. B* **2007**, *111*, 1923–1931. [[CrossRef](#)] [[PubMed](#)]
64. Lu, L.G.; Yu, S.S. Metal distribution in iron-nickel sulfide mineral pentlandite: First-principles study. *Chem. Phys. Lett.* **2019**, *736*, 136786. [[CrossRef](#)]

65. Niu, Y.L.; Langmuir, C.H.; Kinzler, R.J. The origin of abyssal peridotites: A new perspective. *Earth Planet. Sci. Lett.* **1997**, *152*, 251–265. [[CrossRef](#)]
66. Scott, S.R.; Sims, K.W.W.; Frost, B.R.; Kelemen, P.B.; Swapp, S.M. On the hydration of olivine in ultramafic rocks: Implications from Fe isotopes in serpentinites. *Geochim. Cosmochim. Acta* **2017**, *215*, 105–121. [[CrossRef](#)]
67. Niu, Y.L.; Gong, H.M.; Wang, X.H.; Xiao, Y.Y.; Guo, P.Y.; Shao, F.L.; Sun, P.; Chen, S.; Duan, M.; Kong, J.J.; et al. Some key problems on the petrogenesis of seafloor basalts, abyssal peridotites and geodynamics-A non-traditional isotope approach. *Adv. Earth Sci.* **2017**, *32*, 111–127. (In Chinese)
68. Williams, H.M.; Bizimis, M. Iron isotope tracing of mantle heterogeneity within the source regions of oceanic basalts. *Earth Planet. Sci. Lett.* **2014**, *404*, 396–407. [[CrossRef](#)]
69. McDonough, W.F. 3.16-Compositional model for the earth's core. *Treatise Geochem.* **2014**, *2*, 559–576.
70. Poitrasson, F.; Levasseur, S.; Teutsch, N. Significance of iron isotope mineral fractionation in pallasites and iron meteorites for the core-mantle differentiation of terrestrial planets. *Earth Planet. Sci. Lett.* **2005**, *234*, 151–164. [[CrossRef](#)]
71. Bigeleisen, J.; Mayer, M.G. Calculation of equilibrium constants for isotopic exchange reactions. *J. Chem. Phys.* **1947**, *15*, 261–267. [[CrossRef](#)]
72. Urey, H.C. The thermodynamic properties of isotopic substances. *J. Chem. Soc.* **1947**, 562–581. [[CrossRef](#)] [[PubMed](#)]
73. He, Y.; Wu, H.; Ke, S.; Liu, S.A.; Wang, Q. Iron isotopic compositions of adakitic and non-adakitic granitic magmas: Magma compositional control and subtle residual garnet effect. *Geochim. Cosmochim. Acta* **2017**, *203*, 89–102. [[CrossRef](#)]
74. Li, D.Y.; Xiao, Y.L.; Li, W.Y.; Zhu, X.; Williams, H.M.; Li, Y.L. Iron isotopic systematics of UHP eclogites respond to oxidizing fluid during exhumation. *J. Metamorph. Geol.* **2016**, *34*, 987–997. [[CrossRef](#)]
75. Williams, H.M.; Nielsen, S.G.; Renac, C.; Griffin, W.L.; O'Reilly, S.Y.; McCammon, E.A.; Pearson, N.; Viljoen, F.; Alt, J.C.; Halliday, A.N. Fractionation of oxygen and iron isotopes by partial melting processes: Implications for the interpretation of stable isotope signatures in mafic rocks. *Earth Planet. Sci. Lett.* **2009**, *283*, 156–166. [[CrossRef](#)]